



OPEN ACCESS

EDITED BY

Huan Li,
Central South University, China

REVIEWED BY

Mohamed Faisal,
Suez Canal University, Egypt
Shan Liu,
University of South China, China

*CORRESPONDENCE

Junaid Khan,
✉ junaidkhan5615@yahoo.com

RECEIVED 10 April 2025

ACCEPTED 27 May 2025

PUBLISHED 21 July 2025

CITATION

Yu J, Li D, Zheng Y, Ma B, Wang J, Shi G, Xu R, Khan J and Tahir A (2025) Syn-to post-orogenic mineralization in the Shuangkoushan Au–Ag–Pb deposit, North Qaidam: insights from H–O–S isotopes and U–Pb geochronology. *Front. Earth Sci.* 13:1609741. doi: 10.3389/feart.2025.1609741

COPYRIGHT

© 2025 Yu, Li, Zheng, Ma, Wang, Shi, Xu, Khan and Tahir. This is an open-access article distributed under the terms of the [Creative Commons Attribution License \(CC BY\)](https://creativecommons.org/licenses/by/4.0/). The use, distribution or reproduction in other forums is permitted, provided the original author(s) and the copyright owner(s) are credited and that the original publication in this journal is cited, in accordance with accepted academic practice. No use, distribution or reproduction is permitted which does not comply with these terms.

Syn-to post-orogenic mineralization in the Shuangkoushan Au–Ag–Pb deposit, North Qaidam: insights from H–O–S isotopes and U–Pb geochronology

Junzhen Yu^{1,2}, Dexian Li^{1,2}, Youye Zheng^{3,4}, Bo Ma^{1,2}, Jian Wang^{1,2}, Guomei Shi^{1,2}, Rongke Xu⁴, Junaid Khan^{3*} and Asma Tahir⁴

¹State Key Laboratory of Ni and Co Associated Minerals Resources Development and Comprehensive Utilization, Jinchang, Gansu, China, ²Jinchuan Nickel and Cobalt Research and Engineering Institute, Jinchang, Gansu, China, ³School of Earth Resources, China University of Geosciences, Wuhan, China, ⁴Geological Survey Institute, China University of Geosciences, Wuhan, China

The Shuangkoushan Au–Ag–Pb deposits, hosted within meta-basaltic rocks of the Tanjianshan Group in the North Qaidam Orogenic Belt, northwest China, present significant insights into syn-to post-orogenic mineralization processes. Preliminary fluid inclusion studies suggest distinct fluid origins for Ag–Pb and Au mineralization at Shuangkoushan; however, due to the lack of geochronological and isotopic data, as well as comprehensive textural analysis, this hypothesis remains unverified. This research aims to identify the orogenic phase associated with the Shuangkoushan Au and Ag–Pb ore deposits and to constrain the potential sources of the fluid and ore-forming materials through detailed microscopic investigations, zircon U–Pb dating, and H–O–S isotopic analyses. The syn-orogenic meta-basaltic rocks, intruded by gabbros, host numerous orogenic Au deposits and are structurally controlled by a NW–SE-trending ductile shear zone. The contact morphology indicates proximal emplacement of both igneous units, with the influence of the ductile shear zone evident in each assemblage. Geochronological analysis using zircon U–Pb dating of the gabbroic pluton yields a Concordia age of $^{206}\text{Pb}/^{238}\text{U} = 448.5 \pm 2.5$ Ma, which likely predates the formation of the ductile shear zone/quartz veins and provides critical temporal constraints on the Au mineralization sequence. The Au mineralization stage characterized by fluid isotopic compositions ($\delta\text{D}_\text{V-SMOW} = -72.9\%$ to -81.5% ; $\delta^{18}\text{OH}_2\text{O-SMOW} = 3.45\%$ – 4.95% ; $\delta^{18}\text{OV-SMOW} = 10.4\%$ – 13.9%) and pyrite sulfur isotopes ($\delta^{34}\text{S} = +4.8\%$ to $+10\%$), indicating predominantly metamorphic fluids mixed with substantial meteoric water and a basalt-derived metal source. The Ag–Pb ore body formed in association with post-orogenic deep magmatism in late Devonian, rather than the adjacent Neoproterozoic granitic gneisses ($^{206}\text{Pb}/^{238}\text{U} = 835 \pm 6.3$ Ma, 924 ± 6.3 Ma). The Ag–Pb mineralization stage shows H–O ($\delta\text{DV-SMOW} -108.2\%$ to -113.8% , $\delta^{18}\text{OH}_2\text{O-SMOW} 6.45\%$ – 6.55% , $\delta^{18}\text{OV-SMOW} 14.1\%$ – 14.3%) and S-isotopic ($\delta^{34}\text{S} + 0.2\%$ to $+3.3\%$) compositions, suggesting that Ag–Pb mineralizing fluids were primarily sourced from primitive magmatic

water with a minor meteoric water component, and Ag-Pb ore-forming materials were primarily sourced from deep magmatic source. Field geological features, isotopic data, and orogenic deposits comparisons, indicate that the Shuangkoushan Au-Ag-Pb deposit formed through Syn-to Post-orogenic mineralization stages.

KEYWORDS

Tanjianshan metabasalt, Shuangkoushan Au-Ag-Pb deposits, syn-post orogeny, H-O-S isotopes, North Qaidam orogeny

1 Introduction

Orogenic events are critical in forming significant mineral deposits, particularly gold (Au), as these geological processes create conditions conducive to fluid mobilization and metal concentration (Kim and Choi, 2009; Langille et al., 2012). Syn-orogenic mineralization refers to ore-forming processes that occur concurrently with tectonic deformation, commonly resulting in the concentration of Au in structurally controlled settings such as faults, shear zones, and fold hinges, but also in disseminated forms within altered host rocks developed during the same tectonic regime (Oberthür and Weiser, 2008; Sanusi and Amigun, 2020; Cheval-Garabédian et al., 2021). Conversely, post-orogenic mineralization refers to processes that occur after the main compressive tectonic events, often under different temperature and pressure conditions. These settings commonly facilitate the formation of a variety of metal and element deposits—often through hydrothermal processes—such as Ag, Pb, and other base or precious metals (Becker et al., 2009; Yoo and White, 2013; Sun C. et al., 2022).

Mineral assemblages associated with syn-orogenic Au deposits are often characterized by Au-bearing quartz veins formed under metamorphic conditions, whereas post-orogenic Ag-Pb deposits exhibit varying mineralogy, frequently influenced by interactions with meteoric water (Groves et al., 2003; Becker et al., 2009; Yoo and White, 2013). The role of magmatic fluids in driving this evolution is also significant, as they are often enriched in volatile components that can leach metals from surrounding rocks and facilitate deposition in suitable geological settings (Langille et al., 2012; Kalinin et al., 2019). Moreover, the changing conditions associated with tectonic uplift can lead to episodic mineralization events that are distinct but interconnected through their geological history (Kim and Choi, 2009; Becker et al., 2009).

The influence of magmatic and metamorphic processes, as well as the interaction with surface waters, is postulated to affect the isotopic signatures of the minerals formed during these later stages (Jing and Pring, 2019). This duality in mineralization reflects different fluid sources and geochemical environments, suggesting that advanced analytical techniques are necessary to fully capture these transitions and their geochemical implications (Jing and Pring, 2019).

Stable isotope geochemistry is a fundamental analytical tool for constraining the source characteristics, transport mechanisms, and physicochemical conditions of ore-forming fluids, thereby elucidating both the metallogenic processes and evolution of ore-forming fluids (Seo et al., 2006; Yoo and White, 2013; Shi et al., 2024;

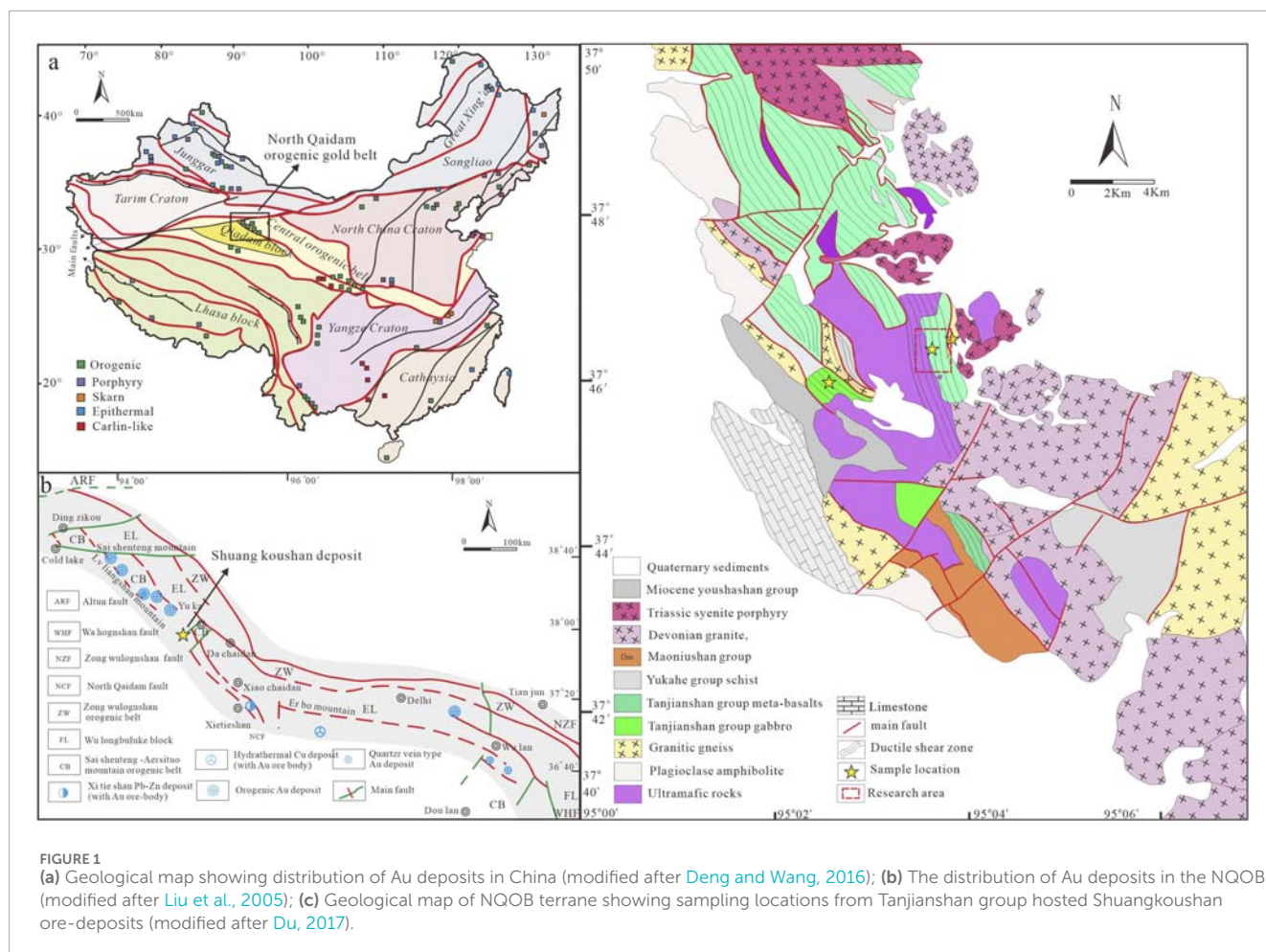
Faisal et al., 2025). Specifically, the examination of hydrogen and oxygen isotopes in quartz veins provides significant insights into the sources of mineral-forming fluids. Similarly, sulfur isotopes ($\delta^{34}\text{S}$) help identify the source of sulfur in the ore-forming fluids, which indirectly constrains the origin of the fluids and biogeochemical processes that control Au incorporation (Kerrick, 1986; Zoheir et al., 2019; Tian et al., 2024). Additionally, zircon U-Pb dating serves as a robust method for determining the timing of geological events (Ito, 2024). This approach helps delineate the temporal relationships between mineral deposits and their host wall rocks, elucidating the complex interactions that occur during tectonic and magmatic processes.

Numerous studies (e.g., Yu et al., 1998) have documented the Shuangkoushan deposit hosted in meta-basaltic rocks of the Tanjianshan group of North Qaidam, which is a significant area for understanding mineralization processes related to geological evolution. The presence of Au-Bi-Te-S deposits and associated mineral assemblages in the region suggests a complex hydrothermal system, indicating that fluid pathways and interaction with host rocks significantly influence the ore body's distribution and composition (Oberthür and Weiser, 2008; Xu et al., 2019). The Shuangkoushan area is a large-scale Ag-Pb producing area that requires further in-depth investigation (Liu and Deying, 2019). Preliminary fluid inclusion studies in ore-bearing quartz veins by Meng (2017) and Yu et al. (2020) suggest that Ag-Pb mineralization is associated with magmatic-hydrothermal activity, while Au mineralization is driven by metamorphic fluids. Yet, due to the lack of geochronological and isotopic data, as well as a comprehensive textural analysis of the ore minerals, this hypothesis remains unjustified. This research aims to constrain the syn-to post-orogenic mineralization processes of the Shuangkoushan Au-Ag-Pb deposits (North Qaidam) by investigating the sources of ore-forming fluids and materials, utilizing zircon U-Pb geochronology, H-O-S isotopic analysis, and textural studies.

2 Geological setting

2.1 Regional geology

The North Qaidam Orogenic Belt (NQOB) is a high-pressure/ultrahigh-pressure (HP/UHP) metamorphic belt located at the northeastern margin of the Qinghai-Tibetan Plateau (Figure 1a). It represents a Paleozoic continental collision zone between the Qaidam Block to the south and the Qilian Block to the north



(Song et al., 2005; Zhang et al., 2008; Chen et al., 2022b; Lin et al., 2025). The NQOB, encompassing the Yeluotuoquan, Qianmeiling, Hongliugou, Tanjianshan, and Yuka areas, are a critical region for orogenic mineral deposits—particularly Au and base metals. These deposits are primarily hosted within specific lithological units, including carbonaceous phyllite and carbonate rocks of the Wandonggou Group and mafic volcanic rocks (metabasalt) of the Tanjianshan Group (Yu et al., 1998; Zhang et al., 2010; Fan, 2016). These deposits are controlled by a NW–SE-trending ductile shear zone, similar to other regional deposits such as the Qinglonggou and Jinlonggou deposits (Liu et al., 2005). Geological structures and magmatic activities have played a crucial role in the formation of polymetallic ore deposits in northwest China (Shi et al., 2004; Shi et al., 2006; Wu et al., 2001; 2007). The exposed stratigraphy comprises a Cambrian–Ordovician greenschist facies, metamorphosed sequence of arc-related volcanic and sedimentary rocks of Tanjianshan Group, Maojiushan sandstone and tuff, Yukahe schist and gneiss (Zhao et al., 2003; Chen et al., 2018a).

The gabbros intrude into the Tanjianshan Group, which consists of low-grade metamorphic volcanic-sedimentary rocks, including metabasalts, metabasaltic andesites, dacites, sericite schists, carbonaceous schists, marbles, metasandstones, and conglomerates (Huichu et al., 2003; Lei et al., 2022). The

Tanjianshan Group contains the Shuangkoushan Au–Ag–Pb ore deposits, adjacent to a Pb–Zn magmatic-hydrothermal deposit and numerous orogenic Au deposits from other complexes in the region (Xietieshan and Luliangshan complexes, respectively; Deng and Wang, 2016; Sun et al., 2017; Cai et al., 2018). The exposed deformation features in the Shuangkoushan area include a NW-trending ductile shear zone, a brittle–ductile shear zone, and a NE-trending brittle fracture system. The formation and localization of the deposit were primarily controlled by these structural features.

2.2 Local geology

The exposed lithologies in the Shuangkoushan area include tonalite, granodiorite, gabbro, mica quartz schist, quartzite, meta-sandstone with associated conglomerates, and Quaternary alluvium (Figure 2a). Additionally, mafic and ultramafic pyroclastic rocks were emplaced along thrust faults, with protolith ages ranging from 450 to 530 Ma (Sun et al., 2019; Cai et al., 2021; Lei et al., 2022; Jiang et al., 2024; Chen et al., 2025). Preliminary drilling has indicated that the Shuangkoushan ore deposit consists of distinct Au and Ag–Pb mineralization bodies, with total reserves exceeding 5 t of Au and 39 t of Ag, along with a significant amount of Pb (Meng, 2017). In the study area, both mineralized bodies are hosted within



metabasaltic rocks of the Tanjianshan Group deposits, located at the western margin between the Xietieshan and Luliangshan complexes (Figures 1b,c). These metabasalts have undergone significant mylonitization and fragmentation (Chen et al., 2018b).

The Au ore body is primarily hosted in a NW–SE trending brittle-ductile shear zone, dipping 50° – 75° to the NW. A total of 10 ore bodies have been identified through exploration, including following main ore bodies number: 10, 9, 4, and 5 with an average grade of 2.24 g/t (Figure 2b). Orebody No. 9 is approximately 172 m long and 3.7 m wide, with an average Au grade of 6.3 g/t. Orebody No. 10 consists of three orebody layers, extending a total of 2 km in length and 60 m in width, with a grade ranging from 1 to 3.8 g/t. Orebody No. 4 is about 700 m long and 2 m wide, with a grade of 1.02–3.6 g/t (Du, 2017). These ores are primarily classified as structurally altered rock and quartz-vein types (Yu et al., 2020). A critical aspect of recent research is the recognition of multistage pyrite formation—classified as Py1, Py2, Py3, and Py4—which plays a key role in constraining the mineralization sequence and fluid evolution. Each generation of pyrite exhibits distinct textural, compositional, and isotopic signatures that correlate with different mineralization stages. Arsenian pyrite (Py1) is the predominant ore mineral in the hypogene ores of area, occurring as subhedral or euhedral fine-grained infillings in quartz fractures (Yu et al., 2020). The gangue minerals mainly include quartz, sericite, and

chlorite (Yu et al., 2020). Au occurs primarily as invisible Au in Py1, with grain sizes ranging from $10\ \mu\text{m}$ to $70\ \mu\text{m}$. The Au size range can be observed in the photograph from the preliminary research work of this area by Chen et al. (2018b). Sulfide minerals appear as disseminations or infilling veinlets within brittle fracture zones and brittle–ductile shear fracture zones, displaying various metamorphic relationships and textures within the alteration zones (Yu et al., 2020). Py2 is porous and coexists with other sulfide minerals (Py1, Py3, etc.). Py2 metasomatized by Py3. Py3 is anhedral and forms in later stages, Py3 further metasomatized by chalcopyrite. The Au grade is positively correlated with pyrite content. Hydrothermal alteration in the Au mineralization stage is characterized by sericitization, silicification, and sulfidation, with no clear zonation.

The Ag–Pb orebodies contain reserves exceeding 39 t of Ag, with an average grade of 343.52 g/t, along with a significant amount of Pb, averaging 11.10% (Meng, 2017). These orebodies are controlled by NE-trending extensional faults and occur as infilling hydrothermal veinlets that cut through the earlier Au ore bodies (Figure 2a). The ore bodies form lens-shaped deposits at the surface and extend to depths greater than 330 m.

The predominant hypogene ore minerals include galena, stromeyerite (AgCuS), and pyrargyrite (Ag_3SbS_3), with minor amounts of chalcopyrite and sphalerite. Galena occurs as fine

subhedral or euhedral grains filling fractures in pyrite (Py4) (Yu et al., 2020). Stromeayerite and pyrargyrite display solid-solution separation textures, typically enclosed by galena (Yu et al., 2020). The gangue minerals consist of quartz, calcite, sericite, and carbonaceous materials (Yu et al., 2020). Sulfide minerals occur as thin infilling veinlets within the brittle fracture zone (Yu et al., 2020). Hydrothermal alteration associated with Ag–Pb mineralization is characterized by silicification, sulfidation, and carbonatization.

3 Analytical methods

3.1 Sample collection

The sample collection site is Shuangkoushan, located in the North Qaidam region of western China. During the field survey, two fresh rock samples were collected: one from the gabbro unit (95°3'0"E, 37°45'36"N) and another from the granitic gneiss unit (95°4'26.4"E, 37°46'12"N), both adjacent to the Shuangkoushan ore deposits for age dating (Figure 1c). An H–O isotope study was conducted on eight quartz samples collected near 95°4'12"E, 37°45'36"N from the Au and Ag–Pb ore bodies. Additionally, ten galena–chalcopyrite-bearing samples from the Ag–Pb ore body, collected from drill holes ZK01 (95°4'12"E, 37°45'36"N) and ZK02 (95°4'33.6"E, 37°43'48"N) (Figure 2a), and twenty-two pyrite-bearing samples from the Au ore body in the vicinity of 95°43'12"E, 37°46'12"N were subjected to *in situ* sulfur isotope analysis (Figure 1c). Approximately six fresh rock samples were also collected from Tanjianshan metabasalts—hosting Au–Ag–Pb deposits—near 95°4'12"E, 37°45'50.4"N for textural studies. Each sample, weighing approximately 1 kg, was placed in a labeled bag with a unique identification number and subsequently dispatched to the laboratory.

3.2 Textural analysis

Sulfide-bearing rock samples were cut, polished to a mirror finish, and carbon-coated to ensure conductivity. A Scanning Electron Microscope (SEM) equipped with a Backscattered Electron (BSE) detector was used at the State Key Laboratory of Geological Processes and Mineral Resources, China University of Geosciences (Wuhan). The SEM was operated at an accelerating voltage of 10–20 kV, with a moderate beam current and a working distance of 10–15 mm. BSE images were formed by detecting electrons backscattered from the sample surface, providing compositional contrast based on atomic number differences. This is crucial for distinguishing between different sulfide phases (Novikov, 2014). High-resolution grayscale images were obtained, clearly revealing the textural relationships among various sulfide phases. For further details on the procedure, refer to Čalkovský et al. (2023).

3.3 Geochronology

Crushing and zircon selection for the Gabbro (SK01) and Granitic Gneiss (GS01) samples were conducted at the

Langfang Institute of Geological and Mineral Research Laboratory. Initially, samples were broken into small fragments, washed, dried, and then pulverized to 200 mesh. Zircons were separated using conventional heavy liquid and magnetic separation techniques, mounted in epoxy resin, and polished to expose grain centers.

Zircons were selected for isotopic analysis based on cathodoluminescence (CL) imaging, performed at the Wuhan Sample Solution Analytical Technology Co., Ltd., using an Analytical Scanning Electron Microscope (JSM-IT100) equipped with a GATAN MINICL system. Imaging was conducted with a 10.0–13.0 kV electric field and an 80–85 μ A tungsten filament.

A total of thirty-five zircon grains underwent U–Pb dating and trace element analysis simultaneously using LA-ICP-MS at Wuhan Sample Solution Analytical Technology Co., Ltd. The laser ablation system consisted of a GeolasPro system, including a COMPexPro 102 ArF excimer laser (193 nm wavelength, 200 mJ maximum energy) and a MicroLas optical system. Ion signal intensities were measured using an Agilent 7700e ICP-MS. Helium was used as a carrier gas, while argon served as the make-up gas, mixed with helium via a T-connector before entering the ICP. A “wire” signal smoothing device was employed (Hu et al., 2015). Zircon 91,500 and glass NIST610 were used as external standards for U–Pb dating and trace element calibration, respectively. Each analysis included background acquisition for ~20–30 s, followed by 50 s of data acquisition. Data processing, including background selection, integration, time-drift correction, and quantitative calibration, was performed using Excel-based ICPMSDataCal software (Liu et al., 2008). Concordia diagrams and weighted mean age calculations were generated using Isoplot/Ex_ver3. The laser ablation system and ICP-MS operating conditions, as well as data reduction methods, followed Zong et al. (2017).

3.4 Oxygen-hydrogen isotope geochemistry

Four quartz samples were collected from the Au ore body and four from the Ag–Pb ore body. Testing was conducted at the Analytical Testing Research Center of the Beijing Institute of Geology. The samples were first crushed, and a preliminary selection to 40–60 mesh was conducted under a stereo microscope to ensure that the quartz mineral purity exceeded 99%. Isotopic analysis was performed using the DZ/T 0184.19-1997 water hydrogen isotope zinc reduction method. This involved drying the samples at a low temperature to remove adsorbed water and then heating to above 600°C to extract water from the fluid inclusions. The extracted water was then reacted with zinc to produce hydrogen, which was analyzed using mass spectrometry.

Oxygen isotopes were measured using the bromine pentafluoride (BrF₅) method following the DZ/T 0184.13-1997 standard for silicate and oxide minerals. In this method, BrF₅ reacts with quartz at 500°C–680°C under vacuum, releasing oxygen, which is then analyzed via mass spectrometry. The analytical precision was $\pm 1\%$ for hydrogen isotopes and $\pm 0.2\%$ for oxygen isotopes.

The homogenization temperature of the fluid inclusions in quartz and the mineral–water oxygen isotopic fractionation equation was used to calculate the $\delta^{18}\text{O}_{\text{H}_2\text{O}}$ value of the fluid. The average temperature of the fluid was taken as the representative value, and the equation used for oxygen isotope equilibrium between quartz and water was: $10^3 \ln \alpha_{\text{quartz-H}_2\text{O}} = \frac{3.42 \times 10^6}{T^2} - 3.40$ (Clayton et al., 1972).

3.5 Sulfur isotope geochemistry

In-situ sulfur isotope analyses of the Au ore body and the Ag–Pb ore body were conducted on drill core samples. Au-bearing pyrite, primarily from the Au mineralization stage, was identified based on deformation intensity, metamorphic characteristics, and cross-cutting relationships observed from deep to shallow levels. Galena and chalcopyrite samples were also primarily collected from the Ag–Pb mineralization stage.

Polished thin sections were prepared, and suitable samples were selected through inspection under a reflected-light microscope. Sulfur isotope analysis was performed using laser ablation multi-collector inductively coupled plasma mass spectrometry (LA-MC-ICP-MS) at the State Key Laboratory of Geological Processes and Mineral Resources, China University of Geosciences (Wuhan). For clean ablation of pure sulfide phases backscattered electron (BSE) imaging also used to identifies zoning, inclusions, grain boundaries, and distinguishes sulfides from gangue minerals.

Sulfide samples were analyzed using a laser spot diameter of 30 μm , a repetition rate of 4 Hz, and a laser energy density of approximately 2.5 J/cm². To address instrumental drift and mass bias, a standard-sample bracketing (SSB) approach was applied, while the use of a femtosecond laser ablation system mitigated matrix effects during sulfur isotope analysis of sulfides, as demonstrated in prior studies (e.g., Zhang et al., 2013; Fu et al., 2017). Data processing for the LA-MC-ICP-MS analysis was performed using Iso-Compass software, following established protocols (Zhang et al., 2020). The analytical precision was $\pm 0.2\%$. For further details on the procedure, refer to Wang et al. (2024).

4 Analytical results

4.1 Zircon U–Pb dating

The detailed analytical results for the zircon U–Pb ages of gabbro (GS01) and granitic gneiss (SKS01) are presented in Supplementary Tables S1, S2, with Concordia diagrams and cathodoluminescence (CL) images shown in Figures 3, 4.

The zircons from GS01 are predominantly rounded or short columnar crystals with length-to-width ratios of 2:1 and exhibit no evidence of metamorphism or post-formation alteration (Figure 4a). In contrast, the zircons from SKS01 are generally long, prismatic, or euhedral, with length-to-width ratios of 2:1 or 3:1 (Figure 4b). The Th/U ratios of these zircons range from 0.23 to 1.14 and 0.03 to 0.4, respectively, consistent with those classified

as magmatic origin (Belousova et al., 2002; Faisal et al., 2020; Phyo et al., 2025a; Phyo et al., 2025b).

A total of seventeen spots on seventeen zircon grains from GS01 were analyzed, yielding a weighted mean $^{206}\text{Pb}/^{238}\text{U}$ age of 448.5 ± 2.5 Ma (MSWD = 0.17; Figure 3a), representing the crystallization age of the Shuangkoushan gabbro intrusion.

For SKS01, eighteen zircon grains were analyzed, forming two distinct age groups. The first group, consisting of 11 measurements, yielded a weighted mean $^{206}\text{Pb}/^{238}\text{U}$ age of 839.8 ± 5 Ma (MSWD = 0.69; Th/U average 0.16). The second group, comprising seven measurements, yielded a weighted mean $^{206}\text{Pb}/^{238}\text{U}$ age of 924 ± 6.3 Ma (MSWD = 0.35; Th/U average 0.17), representing the crystallization age of the granitic gneiss (Figure 3b).

4.2 Hydrogen- oxygen isotopic analysis

The results of the H–O isotopic analysis of quartz veins from the two metallogenic stages are presented in Supplementary Table S3. In the Ag–Pb mineralization stage, $\delta\text{D}_\text{V-SMOW}$ values range from -108.2% to -113.8% , with an average of -110.6% . The $\delta^{18}\text{OH}_2\text{O-SMOW}$ values range from 6.45% to 6.55% , with an average of 6.48% . The $\delta^{18}\text{OV-SMOW}$ values range from 14.1% to 14.3% , with an average of 14.17% . In contrast, during the Au mineralization stage, $\delta\text{D}_\text{V-SMOW}$ values range from -72.9% to -81.5% , with an average of -76.2% . The $\delta^{18}\text{OH}_2\text{O-SMOW}$ values range from 3.45% to 4.95% , with an average of 3.97% . The $\delta^{18}\text{OV-SMOW}$ values range from 10.4% to 13.9% , with an average of 11.9% .

4.3 Sulfur isotopic analysis

The results of the *in situ* sulfur isotope analysis are presented in Supplementary Table S4. The tests were conducted on pyrite, galena, and chalcopyrite from drillhole samples representing different ore-bearing types at varying depths. The isotopic composition of pyrite from the Au mineralization stage shows significant variation, with $\delta^{34}\text{S}$ values ranging from $+4.8\%$ to $+10\%$, averaging $+7.05\%$. Within this dataset: Py1 ranges from $+8.1\%$ to $+10\%$ (average: $+9.3\%$), Py2 ranges from $+5.9\%$ to $+7\%$ (average: $+6.4\%$), and Py3 ranges from $+4.8\%$ to $+5.6\%$ (average: $+5.4\%$).

In contrast, the sulfur isotopic composition exhibits less variation in the Ag–Pb mineralization stage. The $\delta^{34}\text{S}$ values for galena range from $+0.2\%$ to $+2.3\%$ (average: $+1.4\%$), while those for chalcopyrite range from $+1.0\%$ to $+3.3\%$ (average: $+1.9\%$).

4.4 Ore paragenesis

In the Shuangkoushan area, two main mineralization stages and five sub-stages have been identified based on cross-cutting relationships among ore-bearing veinlets, observed mineral textures, and assemblages. These stages (Figure 5) include syn-orogenic Au stage (pre-ore, quartz–pyrite, and polymetallic sulfide stage), and post-orogenic Ag–Pb stage (Ag–Pb stage and

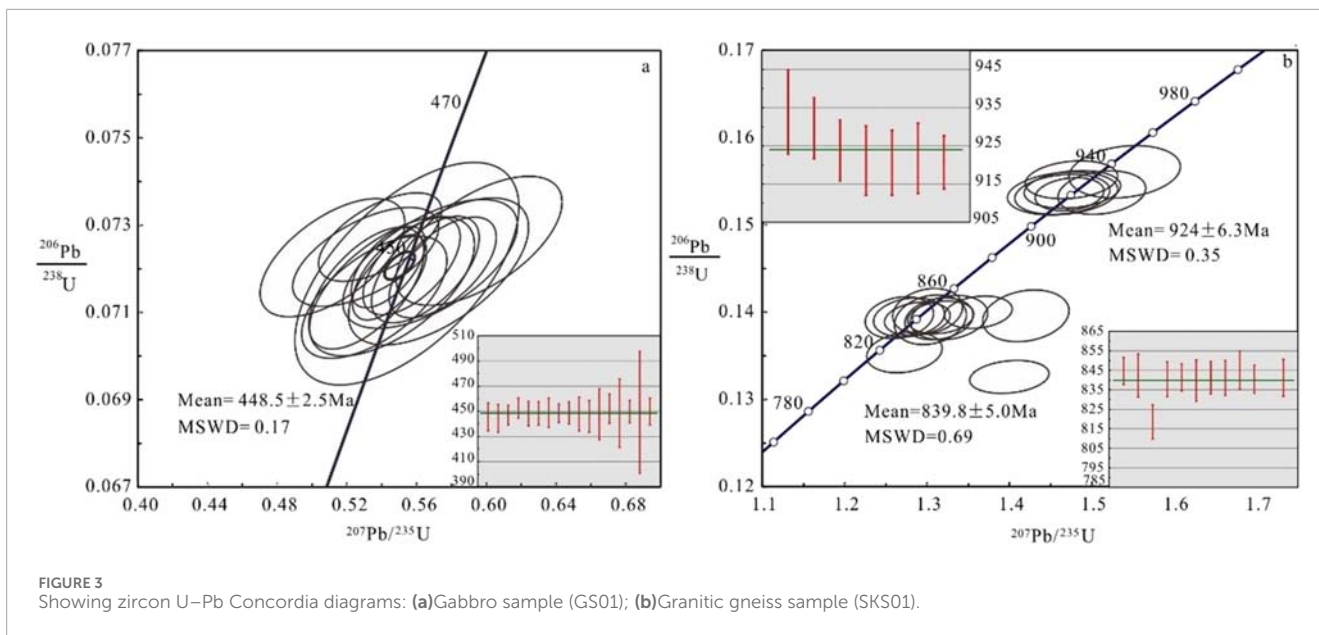


FIGURE 3 Showing zircon U–Pb Concordia diagrams: (a)Gabbro sample (GS01); (b)Granitic gneiss sample (SKS01).

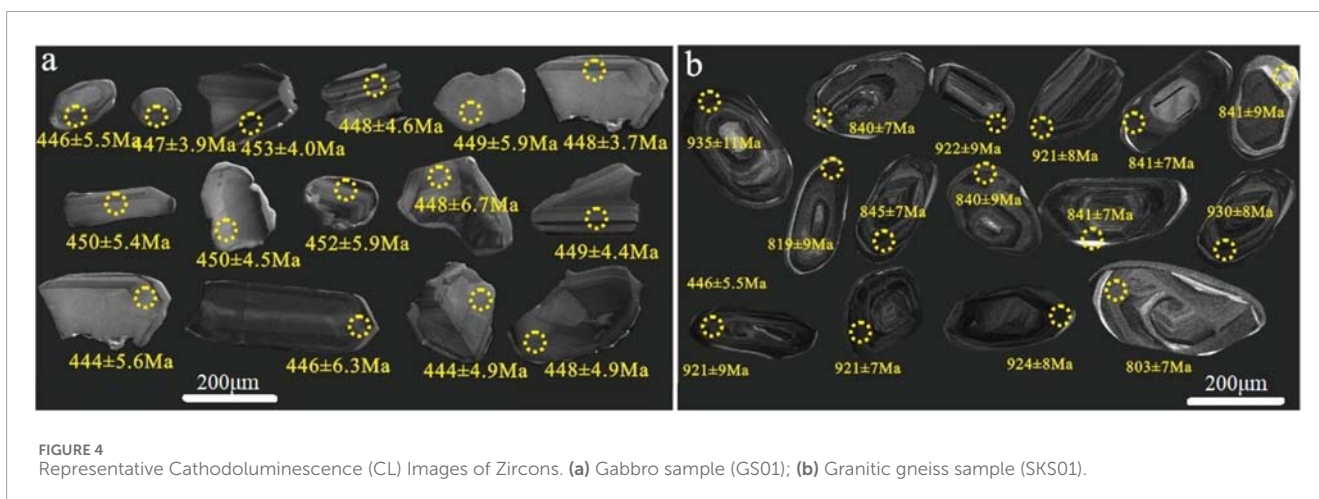


FIGURE 4 Representative Cathodoluminescence (CL) Images of Zircons. (a) Gabbro sample (GS01); (b) Granitic gneiss sample (SKS01).

carbonate stage). Additionally, four types of pyrite were recognized based on textures and paragenetic relationships. During the pre-ore stage (I), the host rocks were subjected to intense tectonic reworking and alteration due to orogenic processes, including strong metamorphism and deformation (Yu et al., 2020). Au-bearing pyrite (Py1) began to pre-enrich the rocks, occurring mainly as fine subhedral grains—either sparsely disseminated or in bamboo-shaped veinlets—within altered mylonites along the shear zone. Some Py1 is intergrown with Py2 in quartz–pyrite veins (stage II), accompanied by gangue minerals such as serpentine, chlorite, epidote, and quartz (Figures 6a,b). Py1 frequently displays evidence of dissolution, metamorphism, and secondary overgrowth from subsequent hydrothermal events. Both Py1 and associated quartz were later crushed, transformed, and metamorphosed by fault activity and hydrothermal overprinting, experiencing both brittle and ductile deformations. Sericite alteration was widespread during this stage. Due to intense structural reworking and alteration, the original composition of the host rocks cannot be accurately determined.

The quartz–pyrite stage (II) represents the main phase of Au mineralization and corresponds to a transition from ductile to brittle deformation structures. Au-bearing pyrite (Py2) is typically subhedral and fine-grained, occurring in disseminated, veinlet-disseminated, and veinlet-type ores hosted in quartz fractures. Py2 often replaces or overgrows Py1 (Figure 6b). Gangue minerals include quartz and sericite. The dominant alteration style during this stage was quartz–pyrite alteration, with minor sericitization (Yu et al., 2020).

By the polymetallic sulfide stage (III), Au mineralization had significantly weakened. The primary minerals were quartz and sericite, with sparse ore minerals including pyrite (Py3) and chalcopyrite. Py2 was overgrown by Py3 (Figure 6c), which was in turn replaced by chalcopyrite. Silicification dominated the alteration assemblage, accompanied by minor pyrite alteration.

The Ag–Pb polymetallic sulfide stage (IV) marks the main phase of Ag–Pb mineralization. The ore bodies occur as veins or lenses that cut across the earlier Au-bearing zones (Figures 6a–c). It can observe in the field photograph from the preliminary

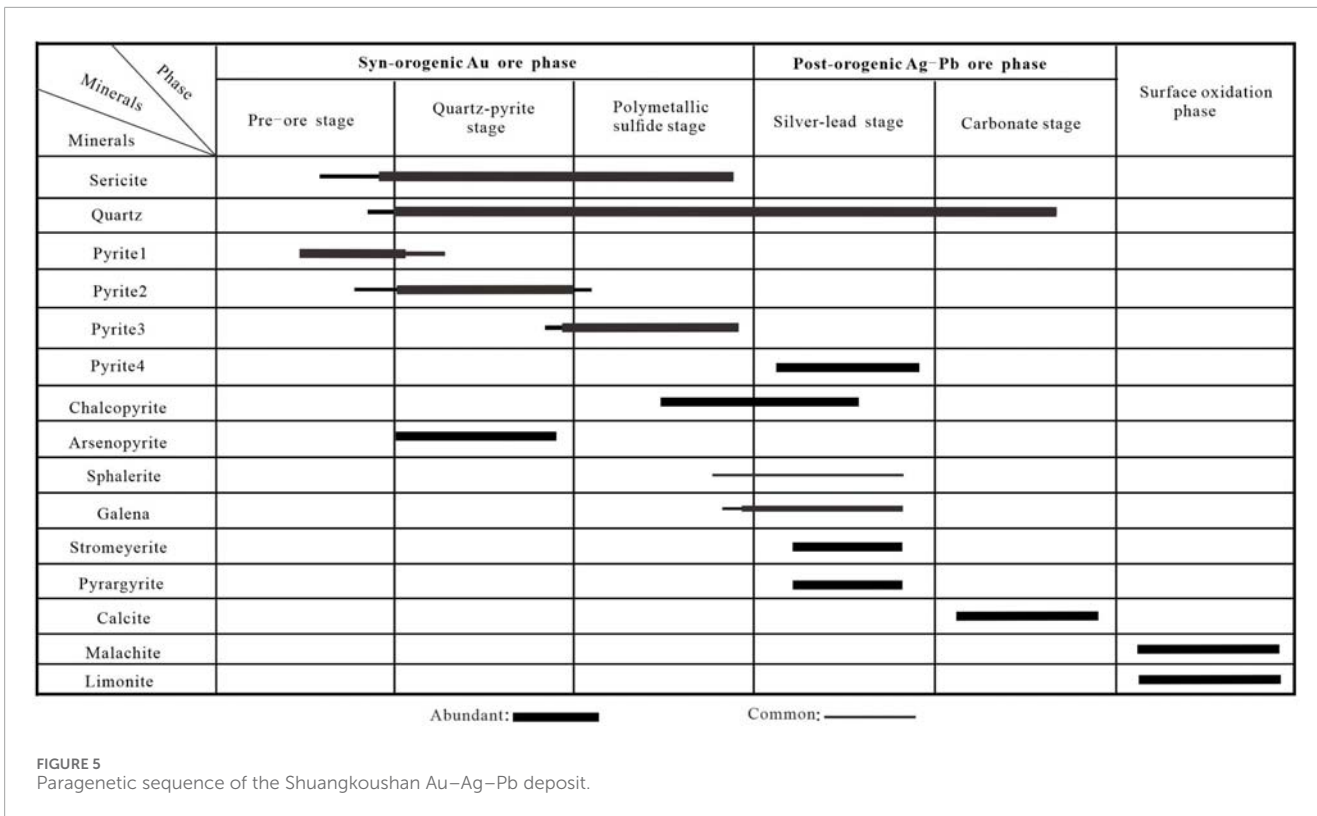


FIGURE 5 Paragenetic sequence of the Shuangkoushan Au-Ag-Pb deposit.

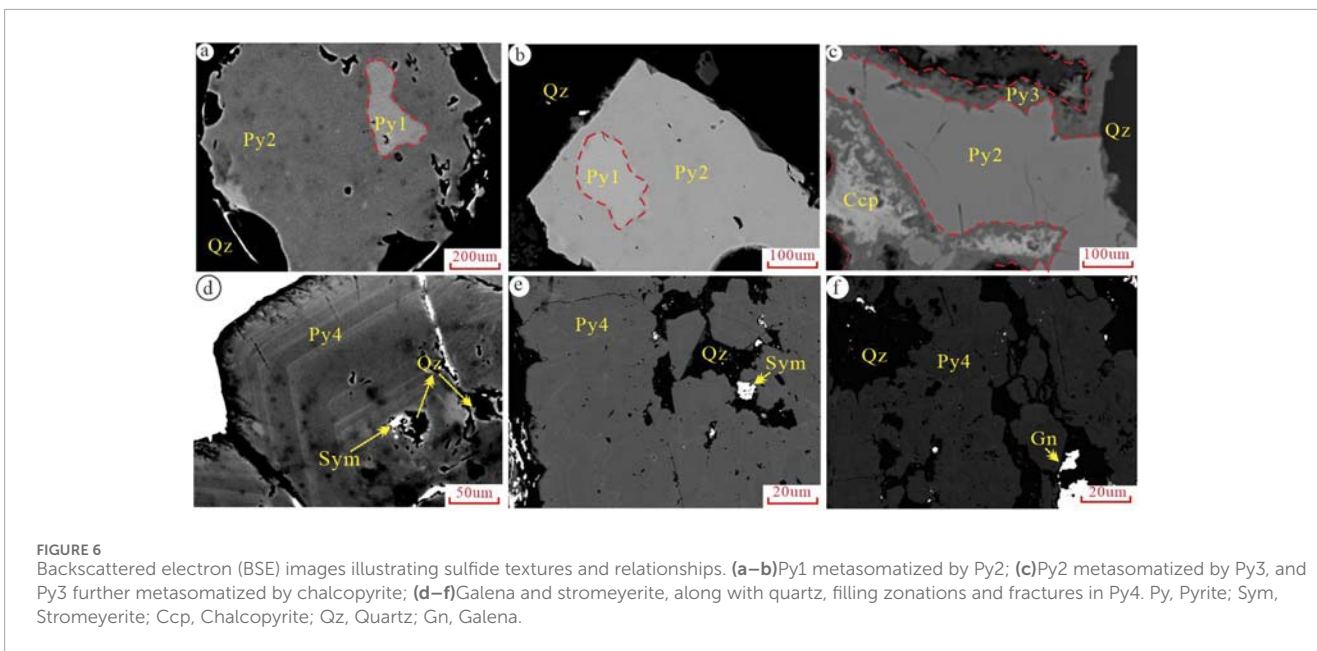


FIGURE 6 Backscattered electron (BSE) images illustrating sulfide textures and relationships. (a–b) Py1 metasomatized by Py2; (c) Py2 metasomatized by Py3, and Py3 further metasomatized by chalcopyrite; (d–f) Galena and stromeyerite, along with quartz, filling zonations and fractures in Py4. Py, Pyrite; Sym, Stromeyerite; Ccp, Chalcopyrite; Qz, Quartz; Gn, Galena.

research work of this area by [Chen et al. \(2018b\)](#). Many Au-bearing breccias were overprinted by Ag-Pb-bearing hydrothermal deposits. Pyrite (Py4) is mostly euhedral and occasionally displays weak zoning ([Figures 6d, e](#)).

In the carbonate stage (V), the mineral assemblage becomes simple in composition, dominated by quartz and calcite, with minor chalcopyrite and pyrite. These sulfides have been partially oxidized to malachite and limonite ([Yu et al., 2020](#)).

5 Discussion

5.1 Syn-orogenic Au to post-orogenic Ag-Pb mineralization

The metallogenic framework of northern Qaidam reflects its dynamic tectonic history. The formation ages of the ore deposits are consistent with the regional tectonic evolution,

encompassing: oceanic subduction (520–460 Ma), continental collision (460–440 Ma), and Continental Exhumation with Orogenic Fluid Modification (430–420 Ma) (Chen et al., 2010; Shuguang et al., 2009; Zhang et al., 2015; Sun et al., 2019). The northern Qaidam margin and East Kunlun Mountains host thirteen structurally controlled Au deposits, each of which formed during successive phases of orogenic activity. The primary episodes of Au mineralization occurred during the Silurian-Triassic periods, with ages ranging from ~425 Ma to ~218 Ma. These ages decrease progressively from north to south (Zhang et al., 2005).

Geochronological data provide critical constraints on the timing of syn-orogenic Au mineralization and its transition to post-orogenic Ag-Pb systems. In the Shuangkoushan area, the formation of the metallic ore body was associated with the metabasaltic rocks of the Tanjianshan Group, which host numerous orogenic Au deposits, all controlled by the NW-SE-trending ductile shear zone of the North Qaidam Orogeny (Zhang et al., 2007). For instance, Fu et al. (2016) measured a sericite Ar-Ar age of 399 ± 4 Ma for the Xitieshan ductile shear zone. Xu et al. (2003) obtained muscovite Ar-Ar ages ranging between 402 Ma and 406 Ma for the Northern Qaidam ultra-high-pressure ductile shear zone (UP = 443–473 Ma and UHP = 420–426 Ma by Shuguang et al., 2009). Zhang et al. (2001) determined a muscovite Ar-Ar age of 401 Ma for the NW-SE-trending ductile shear zone in the Tanjianshan Group. Additionally, Zhang et al. (2007) reported a sericite Ar-Ar age of 409.4 ± 2.3 Ma from the NW-SE-trending ore-controlling shear zone of the Tanjianshan deposit, consistent with the earlier Ar-Ar age of 409 ± 2.3 Ma for metamorphic sericite from the similarly oriented (NW-SE) Au ore-controlling shear zone of the Qinglonggou deposit (Zhang et al., 2005). These ages fall within the period of ductile shear activity, indicating that ductile shear deformation and metamorphism played a major role in the formation of the Au deposits. The Shuangkoushan Au orebodies are also controlled by the NW-SE trending ductile shear zone, suggesting that they may have formed during this time. Furthermore, orogenic Au deposits worldwide are typically interpreted to have formed within collision or accretion zones during peak or late-collision metamorphism (Goldfarb et al., 2001). In this study, we obtained a LA-ICP-MS zircon U-Pb age of 448.5 ± 2.5 Ma for Shuangkoushan gabbro (Figure 3a; Supplementary Table S1), which is likely consistent with the formation age (443 ± 2.9 Ma; Yu et al., 2020) of the Shuangkoushan ore-bearing metabasaltic continental back-arc basin related rocks (Gao et al., 2011; Zhang et al., 2015; Sun et al., 2019). The age of the ductile shear zone and Au-bearing quartz vein (402 ± 4.2 Ma; Yu et al., 2020) in the Shuangkoushan area is younger than that of the host rocks, and therefore likely represents the timing of Au mineralization to some extent.

For the Ag-Pb mineralization stage, work by Xu (2012) on inclusions in galena and sphalerite yielded an Rb-Sr mineralization age of 347.9 ± 3.5 Ma. The zircon U-Pb age obtained for the granitic gneisses is 835 ± 6.3 Ma and 924 ± 6.3 Ma, indicating multistage crystallization (Figure 3b; Supplementary Table S2). These oldest ages represent the continental rifting stage of Rodinia, with corresponding ages (700–850 Ma) discovered by Zhu et al. (2015) on the northern margin of the Qaidam Basin. These results suggest that the Ag-Pb ore-forming fluids and metals were not sourced from the adjacent Neoproterozoic granitic gneiss. The North Qaidam granites age is 386–356 Ma postdate UHP metamorphism (438–420 Ma)

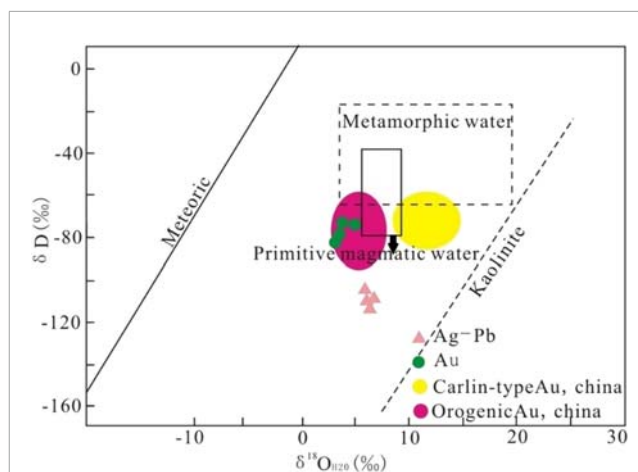


FIGURE 7
Plot of δD versus $\delta^{18}O$ for the ore-forming fluids of the Shuangkoushan Au-Ag-Pb ore field (modified after Sheppard, 1977). Data regarding orogenic Au deposits and Carlin-type Au deposits in China are compiled from multiple sources (Zhang et al., 2000; Shi et al., 2010; Chen et al., 2010; Zhao, 2011; Xue, 2011; Zhang, 2011; Liang et al., 2011; Lu et al., 2011; Fan et al., 2012; Wang, 2012; Xia et al., 2013).

of the deeply subducted continental crust, confirming their post-collisional origin (Sun G. C. et al., 2022).

5.2 Source of ore-forming fluids

Fluids transport thermal energy and ore-bearing minerals in various forms, such as hydrothermal fluids, CO_2 -rich fluids, geothermal fluids, etc., (Deng et al., 2000; Kesler, 2005; Huan-zhang, 2008). Previous studies (Chen et al., 2023) have suggested that multiple fluid sources contribute to the formation of ore deposits: Hydrous fluids liberated by metamorphic dehydration (Yardley and Cleverley, 2015), Magmatic-hydrothermal fluids (Lang and Baker, 2001; Treloar et al., 2015), Deep metamorphic dehydration fluids or magmatic-hydrothermal fluids convecting with meteoric water during uplift (Jenkin et al., 1994), CO_2 -rich fluids released when the mantle interacts with other hydrothermal fluids (Phillips and Evans, 2004). During the Au mineralization stage in the Shuangkoushan area, the values of δD_{V-SMOW} and $\delta^{18}O_{H_2O-SMOW}$ (Supplementary Table S3) are lower than typical values for orogenic Au deposits ($\delta D_{V-SMOW} = -20\text{‰}$ to -80‰ ; $\delta^{18}O_{H_2O-SMOW} = +5\text{‰}$ to $+10\text{‰}$; Kerrich et al., 2000; Zheng and Chen, 2000). In the δD_{V-SMOW} vs. $\delta^{18}O_{H_2O-SMOW}$ plot (Figure 5), the Au samples trend between metamorphic fluids and meteoric water, with values lower than those of typical orogenic Au deposits (Groves et al., 1998; 2003; Goldfarb and Groves, 2015) and local deposits such as Hongliugou (Supplementary Table S5). However, these values align with the variations observed in orogenic Au deposits in China (Zhang, 2011; Fan et al., 2012; Wang, 2012). This suggests that the Au mineralization fluids originated from metamorphic fluids mixed with a substantial meteoric water component. During the Ag-Pb mineralization stage in Shuangkoushan, the samples in the plot trend toward magmatic water alongside meteoric water (Figure 7; Supplementary Table S3). This indicates that Ag-Pb mineralization fluids were sourced primarily from primitive magmatic water with a minor meteoric water component.

5.3 Potential source of Au-Ag-Pb

Previous studies have identified several sources of metals in ore deposits such as metamorphosed rocks (Phillips and Powell, 2010), intrusion-related primary magmatic sources (Lang and Baker, 2001; Hart et al., 2004), carbonaceous, pyrite-rich sedimentary rocks (Daliran, 2007; Gaboury, 2013), and metabasaltic rocks (Augustin et al., 2016). Among these, metabasaltic rocks have a greater potential to serve as a primary source of remobilized Au during the metamorphogenic formation of orogenic Au deposits such as, Wona-Kona Au deposit (Bierlein and Craw, 2009; Augustin and Gaboury, 2017). Evaluating the origins of metals and fluids particularly during the Au mineralization stage, requires identifying the source of sulfur (Chang et al., 2008).

The pyrite $\delta^{34}\text{S}$ values in this study ranging from +4.8‰ to +10.0‰ (Supplementary Table S4), overlap with those of biogenic sulfide ($\delta^{34}\text{S} = 2\text{‰}-46\text{‰}$; Detmers et al., 2001) and metamorphic rocks ($\delta^{34}\text{S} = -20\text{‰}$ to +20‰) but are higher than those of magmatic rocks ($\delta^{34}\text{S} = -1.1\text{‰}-3.5\text{‰}$; McClenaghan, 2013). Previous research has indicated that there is no biological component in sulfides from volcanic rocks and that sulfur concentrations in minerals are largely preserved in ore deposits subjected to metamorphism up to the amphibolite facies. Beyond this stage,

sulfur content increases with the degree of metamorphism, reaching up to 2000 $\mu\text{g/g}$ in amphibolite facies fluids (Rauchenstein-Martinek et al., 2014; Rauchenstein-Martinek et al., 2016). As shown in Supplementary Table S4, the $\delta^{34}\text{S}$ value for pyrite gradually decreases from deep to shallow samples (9.3 \rightarrow 6.9 \rightarrow 6.1 \rightarrow 5.4), correlating with a decrease in metamorphic intensity (Figure 8). Additionally, most orogenic Au deposits in the western part of North Qaidam, including the Yuka, Yeluotuoquan, Qianmeiling, and Hongliugou deposits, exhibit a spatial, temporal, and genetic association with Tanjianshan meta-basaltic rocks. These rocks are favorable for Au mineralization and show positive anomalies in elements such as Ag, As, Au, B, Bi, Sb, Te, and W (Groves et al., 1998). The Tanjianshan meta-basaltic rocks contain higher concentrations of Au, Cr, and Ni (Au: 19.09×10^{-9} ; Cr: 167.40×10^{-6} ; Ni: 64.36×10^{-6}) compared to local average values (Au: 1.35×10^{-9} ; Cr: 55.4×10^{-6} ; Ni: 9.94×10^{-6}). These characteristics are similar to those of Au-bearing greenstone belts worldwide (Henley et al., 1976; McKeag et al., 1989). Together with the deposit geology and H-O isotopic results (Figure 9), these findings suggest that the Au ore-forming material was sourced from the Syn-orogenic meta-basaltic rocks of the Tanjianshan Group, which have relatively high background Au values.

During the Ag-Pb mineralization stage in study area, $\delta^{34}\text{S}$ values for galena range from 0.2‰ to 2.3‰ (Supplementary Table S4),

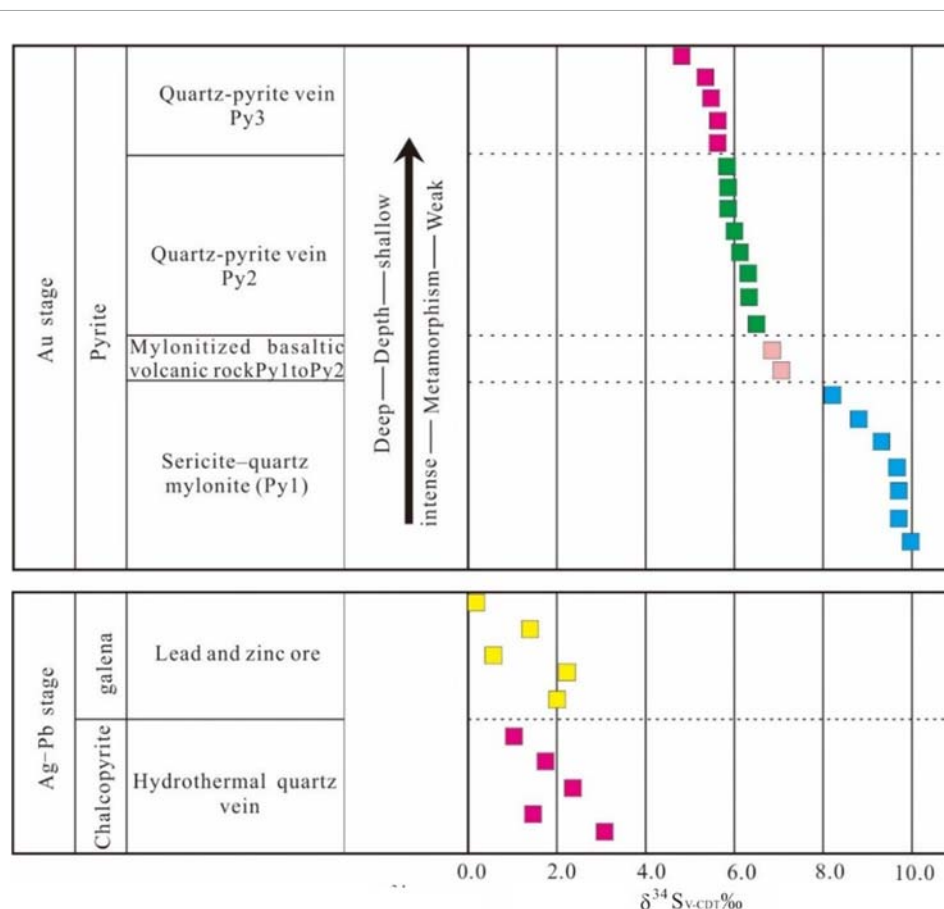
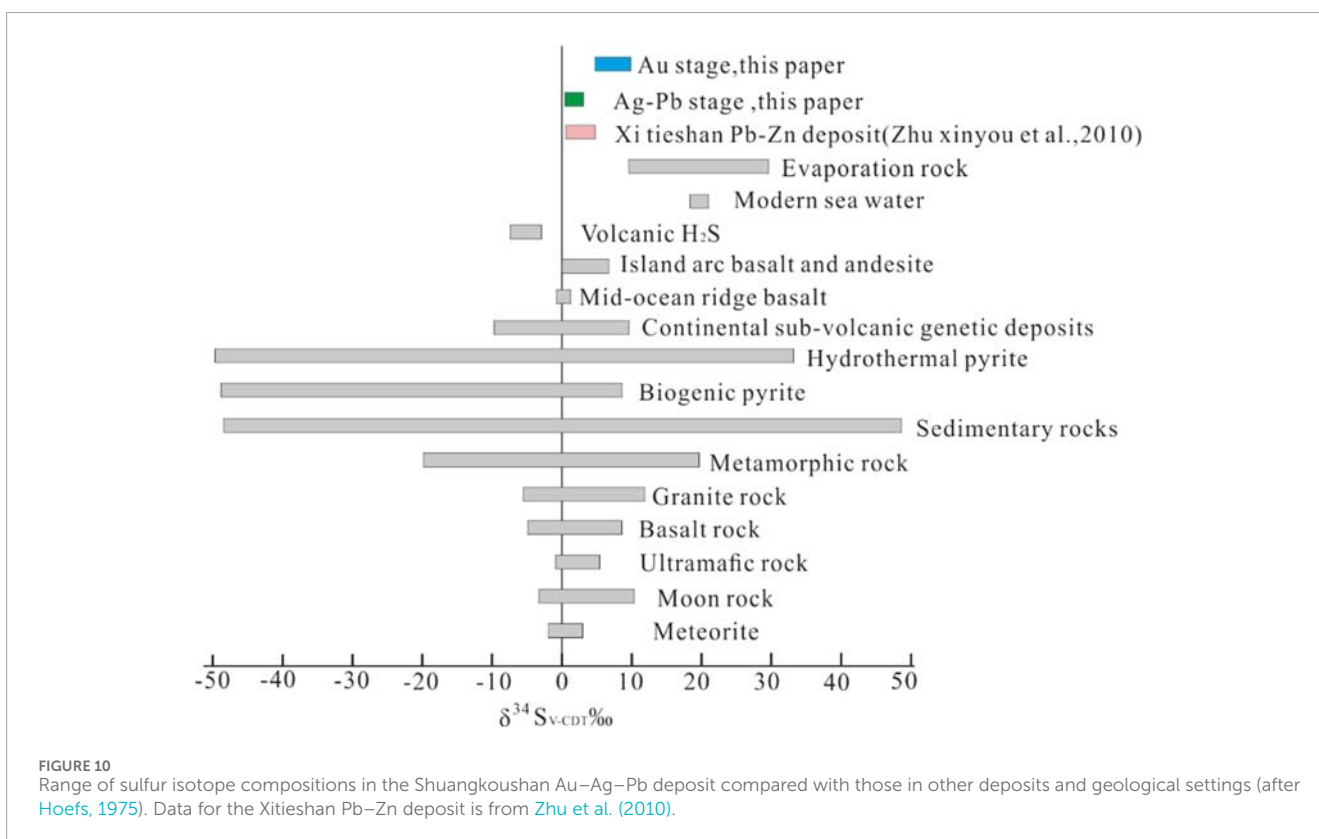
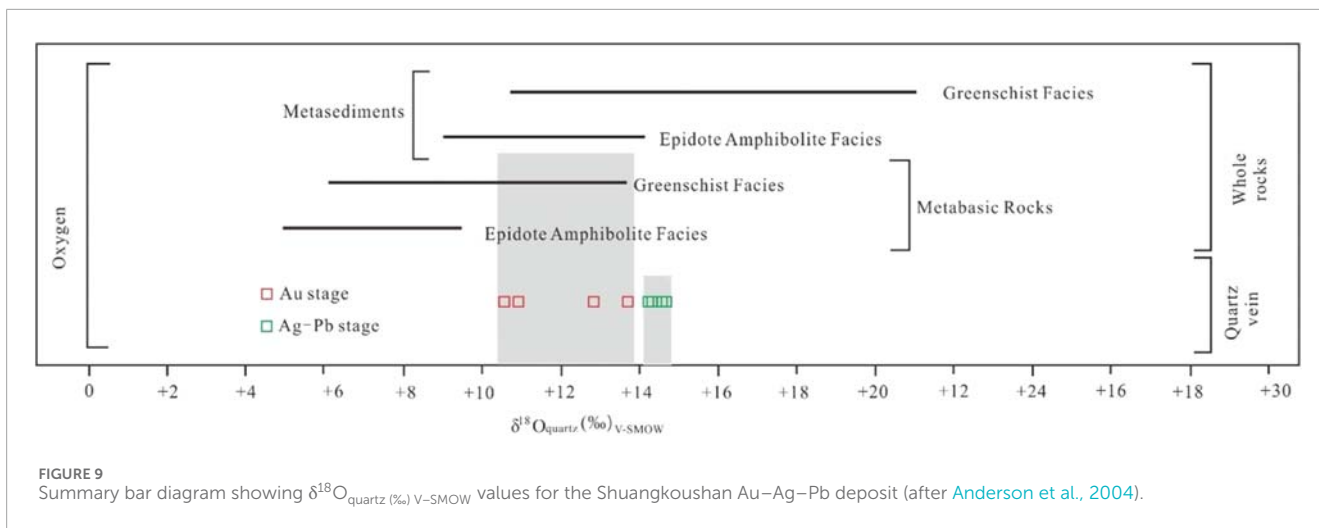


FIGURE 8 Sulfur isotopic composition of pyrite from the Au mineralization stage, and chalcopyrite and galena from the Ag-Pb mineralization stage of the Shuangkoushan Au-Ag-Pb deposits.



while those for chalcopyrite range from 1.0‰ to 3.3‰. These values fall within the typical range of magmatic sulfur ($0\text{‰} \pm 3\text{‰}$; [Chaussidon and Lorand, 1990](#)) and are consistent with those observed in the large-scale Xitieshan Pb–zinc deposits (galena $\delta^{34}\text{S} = 2.0\text{‰}–2.2\text{‰}$; [Wang et al., 2009](#); [Zhu et al., 2010](#); [Figure 10](#)). This suggests that the Ag–Pb ore-forming material was primarily sourced from post-orogenic deep magma or Devonian granite.

5.4 Shuangkoushan Au–Ag–Pb deposit formation

The Qaidam Orogenic Belt is part of the northern margin of the North China Craton and has played a significant role in the formation of the Shuangkoushan Au–Ag–Pb deposit. The belt is characterized by a series of metamorphic and magmatic

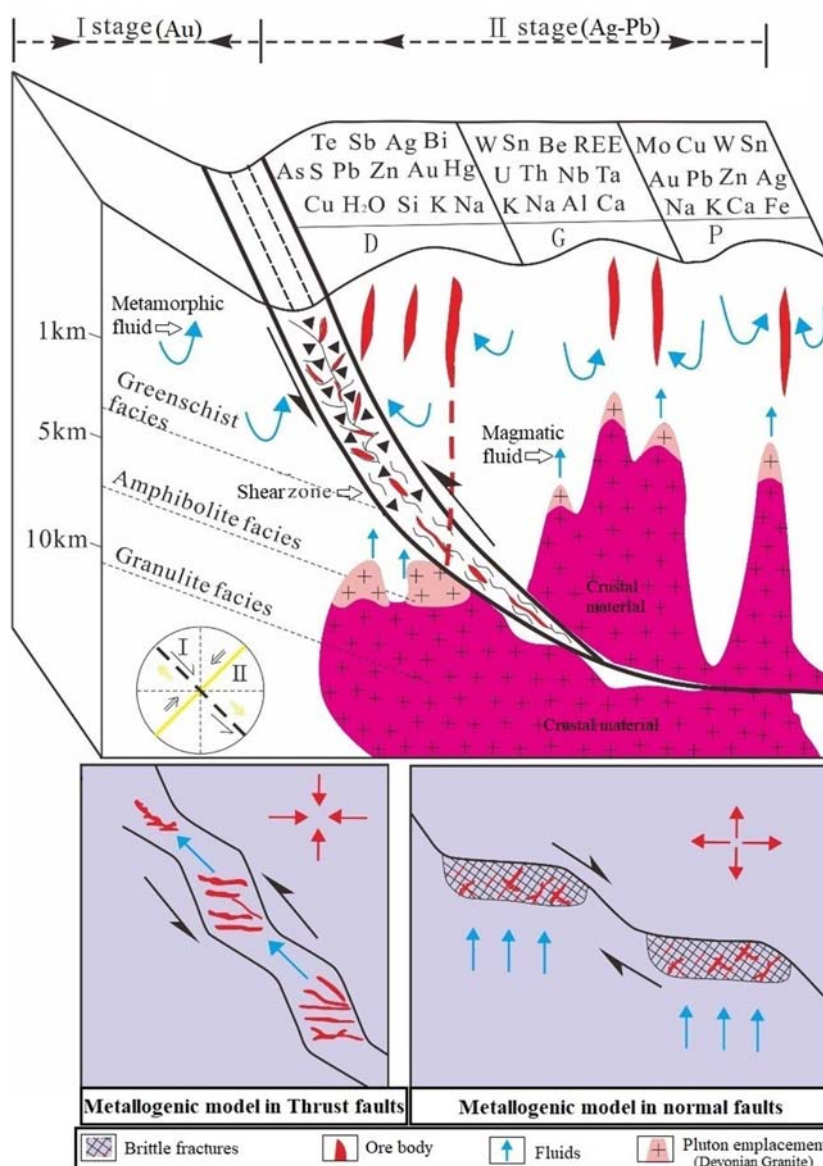


FIGURE 11 Conceptual model of the Shuangkoushan Au–Ag–galena deposit (after Chen, 2013).

rocks, which have been shaped by the tectonic evolution of the region (Yang and Santosh, 2020; Li and Yan, 2023). The geological features, isotopic data, and comparison with orogenic deposits in the Shuangkoushan area (Supplementary Table S5) all indicate that the Au–Ag–Pb deposit formed through two distinct mineralization stages, which separately produced Au and Ag–Pb ore bodies at different times and during different phases (syn- and post-) of the North Qaidam orogeny. The syn-post tectonic framework of the Qaidam Orogenic Belt is a result of multiple tectonic phases, including Cambrian–Ordovician magmatic arc formation, Silurian–Devonian orogeny, Permian–Triassic magmatic arc, and Cenozoic collisional magmatism by UHPM exhumation and collapse (Wang et al., 2014; Chen et al., 2022a; Wang et al., 2023; Wu et al., 2024; Jiang et al., 2025).

The Shuangkoushan Au-ore body is a metamorphic-hydrothermal type deposit genetically associated with syn-orogenic metamorphism and deformation. In contrast, the Ag–Pb ore body is an intrusion-related magmatic-hydrothermal type deposit. It was genetically associated to magmatic activity along extensional faults during the post-collision orogeny. These deposits formed through ore-bearing hydrothermal infill, as ore-bearing magma crystallized and differentiated from deep to shallow depths during the regional post-collision extension period, superseding the earlier Au ore body. The Ag–Pb ore-forming fluids originated from deep magma or Devonian granite.

Based on the results of this study and the regional tectonic background of the area, a conceptual model suggests that the Shuangkoushan deposits underwent a two-stage mineralization process (Figure 11). Stage I: Subduction related Ordovician basaltic

rocks with high background Au values underwent metamorphism and deformation during the syn-orogenic process. As a result, fluids were released through dehydration, extracting Au elements. The Au-bearing fluids ascended along faults. In the ductile to brittle–ductile transition zone, Au precipitated from the fluids and became enriched (Figure 11). Stage II: After regional metamorphism and deformation reached their peak, stress began to relax, leading to detachment along the fault zone. Deep crustal material underwent decompression and partial melting, generating an Ag–Pb-bearing magmatic melt that ascended along fault structures. Crystallization and differentiation occurred near the surface, filling tensile fractures that cut across the earlier Au ore body (Figure 11).

6 Conclusion

The Tanjianshan meta-basaltic rocks host the Shuangkoushan Au–Ag–Pb deposits, located adjacent to gabbro intrusions (448 Ma) and granitic gneisses (835 and 924 Ma) within the North Qaidam Orogenic Belt. In the Shuangkoushan ore bodies, multistage pyrite formation—classified as Py1, Py2, Py3, and Py4—plays a key role in constraining both syn-orogenic Au mineralization (pre-ore (P1), quartz–pyrite (P2), and polymetallic sulfide (P3) stages) and post-orogenic Ag–Pb mineralization (Ag–Pb sulfide (P4) and carbonate stages). The oxygen, hydrogen, and sulfur isotopic compositions of the Shuangkoushan ore bodies support the following conclusions:

- (1) At the stage of Au mineralization, the mineralizing fluids were derived from metamorphic fluids mixed with a substantial meteoric water component, with the ore-forming material sourced from the syn-orogenic basaltic rocks.
- (2) At the stage of Ag–Pb mineralization, the mineralizing fluids originated from primitive magmatic fluids, supplemented by a minor component of meteoric water, with the ore-forming material sourced from post-orogenic deep-seated magma or Devonian granite.

Data availability statement

The original contributions presented in the study are included in the article/supplementary material, further inquiries can be directed to the corresponding author.

Author contributions

JY: Investigation, Writing – original draft. DL: Conceptualization, Methodology, Writing – original draft. YZ: Funding acquisition, Writing – original draft. BM: Conceptualization, Investigation, Methodology, Writing – original draft. JW: Data curation, Project administration, Software,

Writing – original draft. GS: Investigation, Methodology, Writing – original draft. RX: Conceptualization, Data curation, Writing – original draft. JK: Conceptualization, Supervision, Writing – review and editing. AT: Writing – review and editing.

Funding

The author(s) declare that financial support was received for the research and/or publication of this article. This research was financially supported by the Project of the State Key Laboratory of Ni & Co Associated Mineral Resources Development and Comprehensive Utilization (No. JKDGNZ26Z202406), the National Natural Science Foundation of China (Grant Nos. 41230311 and 41572069), and the China Geological Survey Project (Grant No. 12120113032800).

Acknowledgments

We gratefully acknowledge all project members and the State Key Laboratory of Geological Processes and Mineral Resources, China University of Geosciences (Wuhan), for their support.

Conflict of interest

The authors declare that the research was conducted in the absence of any commercial or financial relationships that could be construed as a potential conflict of interest.

Generative AI statement

The author(s) declare that no Generative AI was used in the creation of this manuscript.

Publisher's note

All claims expressed in this article are solely those of the authors and do not necessarily represent those of their affiliated organizations, or those of the publisher, the editors and the reviewers. Any product that may be evaluated in this article, or claim that may be made by its manufacturer, is not guaranteed or endorsed by the publisher.

Supplementary material

The Supplementary Material for this article can be found online at: <https://www.frontiersin.org/articles/10.3389/feart.2025.1609741/full#supplementary-material>

References

- Anderson, R., Graham, C. M., Boyce, A. J., and Fallick, A. E. (2004). Metamorphic and basin fluids in quartz–carbonate–sulfide veins in the SW Scottish Highlands: a stable isotope and fluid inclusion study. *Geofluids* 4 (2), 169–185. doi:10.1111/j.1468-8115.2004.00080.x
- Augustin, J., and Gaboury, D. (2017). Paleoproterozoic plume-related basaltic rocks in the Mana gold district in western Burkina Faso, West Africa: implications for exploration and the source of gold in orogenic deposits. *J. Afr. Earth Sci.* 129, 17–30. doi:10.1016/j.jafrearsci.2016.12.007
- Augustin, J., Gaboury, D., and Crevier, M. (2016). The world-class Wona-Kona gold deposit, Burkina Faso. *Ore Geol. Rev.* 78 (2), 667–672. doi:10.1016/j.oregeorev.2015.10.017
- Becker, M., Stelzner, T., Steinbrück, A., Berger, A., Liu, J., Lerosé, D., et al. (2009). Selectively deposited silver coatings on gold-capped silicon nanowires for surface-enhanced Raman spectroscopy. *ChemPhysChem* 10 (8), 1219–1224. doi:10.1002/cphc.200800809
- Belousova, E. A., Griffin, W. L. Y., and O' Reilly, S. (2002). Igneous zircon: trace element composition as an indicator of source rock type. *Contributions Mineralogy and Petrology* 143 (5), 602–622. doi:10.1007/s00410-002-0364-7
- Bierlein, F. P., and Craw, D. (2009). Petrogenetic character and provenance of metabasalts in the aspiring and torlesse terranes, South Island, New Zealand: implications for the Au endowment of the otago schist? *Chem. Geol.* 260 (3–4), 0–315. doi:10.1016/j.chemgeo.2009.01.016
- Cai, P., Chen, X., Majka, J., Klonowska, I., Jeanneret, P., Xu, R., et al. (2021). Two stages of crust–mantle interaction during oceanic subduction to continental collision: insights from mafic-ultramafic complexes in the North Qaidam orogen. *Gondwana Res.* 89, 247–264. doi:10.1016/j.jgr.2020.08.018
- Cai, P. J., Xu, R. K., Zheng, Y. Y., Chen, X., Liu, J., and Yu, J. Z. (2018). From oceanic subduction to continental collision in North Qaidam: evidence from kaipinggou orogenic M-type peridotite. *Earth Sci.* 43 (8), 28752892.
- Čalkovský, M., Müller, E., and Gerthsen, D. (2023). Quantitative analysis of backscattered-electron contrast in scanning electron microscopy. *J. Microsc.* 289 (1), 32–47. doi:10.1111/jmi.13148
- Chang, Z. S., Large, R. R., and Maslennikov, V. (2008). Sulfur isotopes in sediment-hosted orogenic gold deposits: evidence for an early timing and a seawater sulfur source. *Geology* 36 (12), 971–974. doi:10.1130/G25001A.1
- Chaussidon, M., and Lorand, J. P. (1990). Sulphur isotope composition of orogenic spinel lherzolite massifs from Ariège (North-Eastern Pyrenees, France): an ion microprobe study. *Geochimica Cosmochimica Acta* 54 (10), 2835–2846. doi:10.1016/0016-7037(90)90018-g
- Chen, X., Jiang, S., Palmer, M. R., Schertl, H. P., Cambeses, A., Hernández-Urbe, D., et al. (2023). Tourmaline chemistry, boron, and strontium isotope systematics trace multiple melt–fluid–rock interaction stages in deeply subducted continental crust. *Geochimica et Cosmochimica Acta* 340, 120–140.
- Chen, B. J., Wen, C. Q., Huo, Y., Cao, S. Y., Song, F. Z., and Zhou, Y. (2010). Study on fluid inclusions in the Shui Yingdong Au deposit in southwestern of Guizhou province. *Bull. Mineralogy, Petrology Geochem.* 29 (1), 45–51.
- Chen, X., Schertl, H. P., Cambeses, A., Hart, E., Lin, C., Xu, R., et al. (2022b). Cyclicity of multistage anatexis of deeply subducted continental crust during the North Qaidam orogeny: tracing the source, timescale, and evolution of pulsed melts. *Am. J. Sci.* 322 (2), 225–279. doi:10.2475/02.2022.05
- Chen, X., Schertl, H. P., Hart, E., Majka, J., Cambeses, A., Hernández-Urbe, D., et al. (2022a). Mobilization and fractionation of Ti–Nb–Ta during exhumation of deeply subducted continental crust. *Geochimica et Cosmochimica Acta* 319, 271–295.
- Chen, X., Schertl, H. P., Khan, J., Cai, P., Lian, D., Wang, J., et al. (2025). Scandium mineralization during ultramafic-mafic magmatism in the subduction zone. *Chem. Geol.* 673, 122556.
- Chen, X., Xu, R., Zheng, Y., Jiang, X., and Du, W. (2018b). Identifying potential Au–Pb–Ag mineralization in SE Shuangkoushan, North Qaidam, Western China: combined log-ratio approach and singularity mapping. *J. Geochem. Explor.* 189, 109–121. doi:10.1016/j.jgexplo.2017.04.001
- Chen, X., Xu, R. K., Zheng, Y. Y., and Cai, P. J. (2018a). Petrology and geochemistry of high niobium eclogite in the North Qaidam orogen, Western China: implications for an eclogite facies metamorphosed island arc slice. *J. Asian Earth Sci.* 164, 380–397. doi:10.1016/j.jseaes.2018.07.003
- Chen, Y. J. (2013). The creation and application of continental collision metallogenic theory. *Acta Petrol. Sin.* 29 (1), 1–17.
- Cheval-Garabédian, F., Faure, M., Marcoux, É., and Poujol, M. (2021). The tungsten–Au veins of Bonnac (French Massif Central): new constraints for a Variscan granite-related genesis. *Bull. Société Géologique Fr. – Earth Sci. Bull.* 192 (1), 7. doi:10.1051/bsgf/2020041
- Clayton, R. N., O'neil, J. R., and Mayeda, T. K. (1972). Oxygen isotope exchange between quartz and water. *J. Geophys. Res.* B77, 3057–3067. doi:10.1029/JB077i017p03057
- Cui, Y. H., Zhang, D. Q., Li, D. X., Gu, G. X., and Feng, C. Y. (2000). Geological geochemistry and genetic mechanism of the Tanjianshan Au deposit. *Depos. Geol.* 19 (3), 211–221.
- Daliran, F. (2007). The carbonate rock-hosted epithermal gold deposit of Agdarreh, Takab geothermal field, NW Iran—hydrothermal alteration and mineralisation. *Mineral. Deposita* 43 (4), 383–404. doi:10.1007/s00126-007-0167-x
- Deng, J., and Wang, Q. (2016). Gold mineralization in China: metallogenic provinces, deposit types and tectonic framework. *Gondwana Res.* 36, 219–274. doi:10.1016/j.gr.2015.10.003
- Deng, J., Yang, L. Q., Sun, L., Peng, R. M., Chen, X. M., and Du, Z. T. (2000). Ore-Forming dynamics of tectonic regime transformation and multi-layer fluid circulation. *Earth Sci.* 25 (4), 397–403.
- Detmers, J., Brüchert, V., Habicht, K. S., and Kuever, J. (2001). Diversity of sulfur isotope fractionations by sulfate-reducing prokaryotes. *Appl. Environ. Microbiol.* 67, 888–894. doi:10.1128/AEM.67.2.888-894.2001
- Du, W. Y. (2017). *Characteristics of ore-controlling and metallogenic prediction of Au–Ag–Pb deposits in Shuangkoushan area, North Qaidam*. Wuhan: China University of Geosciences.
- Faisal, M., Li, H., Heritier, R. S.N. N., Gul, M. A., Khedr, F. A., Zhou, Z., et al. (2025). Geological and geochemical evolution of the Derhib sulfide-talc deposit in the South Eastern Desert, Egypt: insights into ore genesis and metasomatic alteration. *Lithos* 504–505, 108049. doi:10.1016/j.lithos.2025.108049
- Faisal, M., Yang, X., Khalifa, I. H., Amuda, A. K., and Sun, C. (2020). Geochronology and geochemistry of Neoproterozoic Hamamid metavolcanics hosting largest volcanogenic massive sulfide deposits in Eastern Desert of Egypt: implications for petrogenesis and tectonic evolution. *Precambrian Res.* 344, 105751. doi:10.1016/j.precamres.2020.105751
- Fan, S. L., He, M. C., Yao, S. Z., and Ding, Z. J. (2012). Fluid inclusions and stable isotope geochemistry of Dongchuang Au deposit in western Henan: implications for genesis. *Depos. Geol.* 31 (1), 27–40.
- Fan, X. B. (2016). *Discussion on the genesis of Yuka Au deposit in dachaidan town, Qinghai province*. Wuhan: China University of Geosciences.
- Fu, J., Hu, Z., Li, J., Yang, L., Zhang, W., Liu, Y., et al. (2017). Accurate determination of sulfur isotopes ($\delta^{33}\text{S}$ and $\delta^{34}\text{S}$) in sulfides and elemental sulfur by femtosecond laser ablation MC-ICP-MS with non-matrix matched calibration. *J. Anal. Atomic Spectrom.* 32, 2341–2351. doi:10.1039/C7JA00282C
- Fu, J. G., Liang, X. Q., and Wang, C. (2016). Basic characteristics and formation age of the Xitieshan ductile shear zone, North Qaidam. *Geotect. metallogeny* 40 (1), 14–27.
- Gaboury, D. (2013). Does Au in orogenic deposits come from pyrite in deeply buried carbon-rich sediments? Insight from volatiles in fluid inclusions. *Geology* 41 (12), 1207–1210. doi:10.1130/G34788.1
- Gao, X. F., Xiao, P. X., and Jia, Q. Z. (2011). Redetermination of the Tanjianshan Group: geochronological and geochemical evidence of basalts from the margin of the Qaidam basin. *Acta Geol. Sin.* 85 (9), 1452–1463.
- Goldfarb, R. J., and Groves, D. I. (2015). Orogenic gold: common or evolving fluid and metal sources through time. *Lithos* 233, 2–26. doi:10.1016/j.lithos.2015.07.011
- Goldfarb, R. J., Groves, D. I., and Gardoll, S. (2001). Orogenic gold and geologic time: a global synthesis. *Ore Geol. Rev.* 18 (1), 1–75. doi:10.1016/S0169-1368(01)00016-6
- Groves, D. I., Goldfarb, R. J., Gebre-Mariam, M., Hagemann, S. G., and Robert, F. (1998). Orogenic gold deposits: a proposed classification in the context of their crustal distribution and relationship to other gold deposit types. *Ore Geol. Rev.* 13 (1–5), 7–27. doi:10.1016/S0169-1368(97)00012-7
- Groves, D. I., Goldfarb, R. J., Robert, F., and Hart, C. J. (2003). Gold deposits in metamorphic belts: overview of current Understanding, Outstanding problems, future research, and exploration significance. *Econ. Geol.* 98, 1–29. doi:10.2113/gsecongeo.98.1.1
- Hart, C. J. R., Mair, J. L., Goldfarb, R. J., and Groves, D. I. (2004). Source and redox controls on metallogenic variations in intrusion-related ore systems, tombstone-tungsten belt, yukon territory, Canada. *Earth Environ. Sci. Trans. R. Soc. Edinb.* 95 (1), 339–356. doi:10.1017/S0263593300001115
- Henley, R. W., Norris, R. J., and Paterson, C. J. (1976). Multistage ore genesis in the New-Zealand geosyncline: a history of post-metamorphic lode emplacement. *Miner. Deposita* 11 (2), 180–196. doi:10.1007/BF00204480
- Hoefs, D. J. (1975). Geochemistry of stable isotopes. *Angew. Chem. Int. Ed.* 14 (2), 75–79. doi:10.1002/anie.197500751
- Hu, Z. C., Zhang, W., Liu, Y. S., Gao, S., Li, M., Zong, K. Q., et al. (2015). “Wave” signal-smoothing and mercury-removing device for laser ablation quadrupole and multiple collector ICPMS analysis: application to lead isotope analysis. *Anal. Chem.* 87 (2), 1152–1157. doi:10.1021/ac503749k
- Huan zhang, L. (2008). Role of CO₂ fluid in the formation of gold deposits: fluid inclusion evidences. *Geochimica* 37 (4), 321–328.

- Huichu, W., Songnian, L., Guibang, Y., Houtian, X., Baohua, Z., Qinghai, W., et al. (2003). Tectonic setting and age of the Tanjianshan Group on the northern margin of the Qaidam basin. *Geol. Bull. China* 22 (7), 487–493.
- Ito, H. (2024). Simultaneous U–Pb and U–Th dating using LA-ICP-MS for young (<0.4 ma) minerals: a reappraisal of the double dating approach. *Minerals* 14 (4), 436. doi:10.3390/min14040436
- Jenkin, G. R. T., Craw, D., and Fallick, A. E. (1994). Stable isotopic and fluid inclusion evidence for meteoric fluid penetration into an active mountain belt: alpine schist, New Zealand. *J. Metamorph. Geol.* 12 (4), 429–444. doi:10.1111/j.1525-1314.1994.tb00033.x
- Jing, Z., and Pring, A. (2019). Mineral transformations in gold–(silver) tellurides in the presence of fluids: nature and experiment. *Minerals* 9 (3), 167. doi:10.3390/min9030167
- Jiang, X., Chen, X., Jiang, S., Hoare, L., Zhang, W., Lian, D., et al. (2024). Immiscibility of carbonatitic and alkaline silicate melts from an evolved ultramafic magma: titanite geochronology and in-situ TiNd isotope insights. *Chem. Geol.* 670, 122433.
- Jiang, X., Chen, X., Schertl, H. P., Hoare, L., Cambeses, B., Uribe, D. H., et al. (2025). Rutile petrochronology and titanium isotope compositions record multiple melt–fluid–rock interactions in a continental subduction zone. *Geochimica et Cosmochimica Acta*.
- Kalinin, A. A., Savchenko, Y. E., and Selivanova, E. A. (2019). Mustard gold in the oleninskoe gold deposit, kolmozero–voronya greenstone belt, Kola Peninsula, Russia. *Minerals* 9 (12), 786. doi:10.3390/min9120786
- Kerrick, R. (1986). The stable isotope geochemistry of Au–Ag vein deposits in metamorphic rocks. *Mineral. Assoc. Can. Short. Course Handb.* 13, 287–336.
- Kerrick, R., Goldfarb, R., Groves, D., Garwin, S., and Jia, Y. F. (2000). The characteristics, origins, and geodynamic settings of supergiant gold metallogenic provinces. *Sci. China (Series D)* 43 (Suppl. 1), 1–68. doi:10.1007/BF02911933
- Kesler, S. E. (2005). Ore-forming fluids. *Elements* 1 (1), 13–18. doi:10.2113/gselements.1.1.13
- Kim, C., and Choi, S. (2009). Potassium–argon ages of the epithermal gold–silver mineralization in the haenam–jindo area, Southwestern Korea. *Resour. Geol.* 59 (4), 415–421. doi:10.1111/j.1751-3928.2009.00108.x
- Lang, J. R., and Baker, T. (2001). Intrusion-related gold systems: the present level of understanding. *Mineral. Deposita* 36 (6), 477–489. doi:10.1007/s001260100184
- Langille, M., Personick, M., Zhang, J., and Mirkin, C. (2012). Defining rules for the shape evolution of gold nanoparticles. *J. Am. Chem. Soc.* 134 (35), 14542–14554. doi:10.1021/ja305245g
- Lei, C. H. E. N., Zhen, Y. A. N., and ChangLei, F. U. (2022). Sedimentary environment and tectonic setting of the clastic formation of the Tanjianshan Group in the Tuomoeirite area, North Qaidam. *Acta Petrol. Sin.* 38 (3), 777–792. doi:10.18654/1000-0569/2022.03.11
- Li, C., and Yan, J. (2023). Tectono-magmatic control on the intensity of decratonic gold mineralization in the southeastern margin of the North China Craton: a perspective from geochemical comparison. *Int. Geol. Rev.* 66 (2), 582–606. doi:10.1080/00206814.2023.2202245
- Liang, Y. H., Sun, X. M., Shi, G. Y., Hu, B. M., Zhou, F., Wei, H. X., et al. (2011). Ore-forming fluid geochemistry and genesis of Laowangzhai large scale orogenic Au deposit in Ailaoshan Au belt, Yunnan Province, China. *Acta Petrol. Sin.* 27 (9), 2533–2540.
- Lin, Y., Yu, C., Chen, S., Shi, S., Luo, S., and Khan, J. (2025). Paleozoic multi-stage magmatism in the Yuka terrane, North Qaidam orogenic belt: mantle modification, tectonic evolution, and geodynamic processes. *Front. Earth Sci.* 13, 1545127. doi:10.3389/feart.2025.1545127
- Liu, J., and Deying, D. (2019). Geological characteristics and ore-controlling factors of Shuangkoushan lead–silver deposit in Qinghai Province. *World Nonferrous Met.* (6), 123–125. doi:10.3969/j.issn.1002-5065.2019.06.063
- Liu, Y. S., Hu, Z. C., Gao, S., Gu'nther, D., Xu, J., Gao, C. G., et al. (2008). *In situ* analysis of major and trace elements of anhydrous minerals by LA-ICP-MS without applying an internal standard. *Chem. Geol.* 257 (1–2), 34–43. doi:10.1016/j.chemgeo.2008.08.004
- Liu, Z. T., Ren, J. Q., Yang, Y. Z., and Sun, C. R. (2005). *Au deposits in Qinghai*. Beijing: Geological Publishing House.
- Lu, L. N., Fan, H. R., Hu, F. F., Yang, K. F., Zheng, X. L., and Zhao, H. (2011). Ore forming fluids and genesis of Xin cheng Au deposit in northwestern Jiaodong Peninsula. *Depos. Geol.* 30 (3), 522–532.
- McClenaghan, L. (2013). *Geology and genesis of the Newton bulk-tonnage gold-silver deposit central British Columbia*. (doctoral dissertation). University of British Columbia, Canada
- McKeag, S. A., Craw, D., and Norris, R. J. (1989). Origin and deposition of a graphitic schist-hosted metamorphogenic Au–W deposit, Macraes, East Otago, New Zealand. *Miner. Deposita* 24 (2), 124–131. doi:10.1007/BF00206316
- Meng, H. (2017). *Study on genesis of the Au–Ag–Pb deposit in northern shuang koushan, da chaidan, Qinghai province*. Wuhan: China University of Geosciences.
- Novikov, Y. A. (2014). Backscattered electron imaging of micro- and nanostructures: 1. Method of analysis. *J. Surf. Investigation. X-ray, Synchrotron Neutron Tech.* 8 (4), 775–786. doi:10.1134/s1027451014040296
- Oberthür, T., and Weiser, T. (2008). Gold–bismuth–telluride–sulphide assemblages at the viceroy mine, harare–bindura–shamva greenstone belt, Zimbabwe. *Mineral. Mag.* 72 (4), 953–970. doi:10.1180/minmag.2008.072.4.953
- Phillips, G. N., and Evans, K. (2004). A Role of CO₂ in the formation of Au deposits. *Nature* 429 (6994), 860–863. doi:10.1038/nature02644
- Phillips, G. N., and Powell, R. (2010). Formation of gold deposits: a metamorphic devolatilization model. *J. Metamorph. Geol.* 28 (6), 689–718. doi:10.1111/j.1525-1314.2010.00887.x
- Phyo, A. P., Li, H., Hu, X.-J., Ghaderi, M., Myint, A. Z., and Faisal, M. (2025a). Geology, geochemistry, and zircon U–Pb geochronology of the Nanthila and Pedet granites in the Myeik Sn–W district, Tanintharyi region, southern Myanmar. *Ore Geol. Rev.* 178, 106488. doi:10.1016/j.oregeorev.2025.106488
- Phyo, A. P., Li, H., Myint, A. Z., Hu, X.-J., and Faisal, M. (2025b). Geochronology and petrogenesis of late triassic–early jurassic LCT pegmatites from the Yamon–Kazat area, southern Myanmar: implications for magmatic evolution. *Ore Geol. Rev.* 181, 106633. doi:10.1016/j.oregeorev.2025.106633
- Rauchenstein–Martinek, K., Wagner, T., Wälle, M., and Heinrich, C. A. (2014). Au concentrations in metamorphic fluids: a LA-ICPMS study of fluid inclusions from the Alpine orogenic belt. *Chem. Geol.* 385, 70–83. doi:10.1016/j.chemgeo.2014.07.018
- Rauchenstein–Martinek, K., Wagner, T., Wälle, M., Heinrich, C. A., and Arlt, T. (2016). Chemical evolution of metamorphic fluids in the Central Alps, Switzerland: insight from LA-ICPMS analysis of fluid inclusions. *Geofluids* 16 (5), 877–908. doi:10.1111/gfl.12194
- Sanusi, S., and Amigun, J. (2020). Structural and hydrothermal alteration mapping related to orogenic gold mineralization in part of Kushaka schist belt, North-central Nigeria, using airborne magnetic and gamma-ray spectrometry data. *Sn Appl. Sci.* 2 (9), 1591. doi:10.1007/s42452-020-03435-1
- Seo, D., Park, J., and Song, H. (2006). Polyhedral gold nanocrystals with O_h Symmetry: from octahedra to cubes. *J. Am. Chem. Soc.* 128 (46), 14863–14870. doi:10.1021/ja062892u
- Sheppard, S. M. P. (1977). The Cornubian batholith, SW England. D/H and ¹⁸O/¹⁶O studies of kaolinite and other alteration minerals. *J. Geol. Soc. Lond.* 133 (6), 573–591. doi:10.1144/gsjgs.133.6.0573
- Shi, D., Fan, S., Li, G., Zhu, Y., Yan, Q., Jia, M., et al. (2024). Genesis of Yongping copper deposit in the Qin–Hang Metallogenic Belt, SE China: insights from sulfide geochemistry and sulfur isotopic data. *Ore Geol. Rev.* 173, 106231. doi:10.1016/j.oregeorev.2024.106231
- Shi, G. Y., Sun, X. M., Zhang, Y., Xiong, D. X., Zhai, W., Pan, W. J., et al. (2010). H–O–C–S isotopic compositions of ore-forming fluids in Daping Au deposit in Ailaoshan Au belt, Yunnan Province, China. *Acta Petrol. Sin.* 26 (6), 1751–1759.
- Shi, R. D., Yang, J. S., Wu, C. L., Iizukab, T., and Takafumi, H. (2006). Island arc volcanic rocks in the North Qaidam UHP belt, northern Tibet plateau: evidence for ocean–continent subduction preceding continent–continent subduction. *J. Asian Earth Sci.* 28 (2–3), 0–159. doi:10.1016/j.jseas.2005.09.019
- Shi, R. D., Yang, J. S., Wu, C. L., Tsuyoshi, I., and Takafumi, H. (2004). Island arc volcanic rocks in the ultrahigh pressure metamorphic belt, North Qaidam. *J. Geol.* 78 (1), 52–64.
- Shuguang, S., Yaoling, N., Lifei, Z., and Guibin, Z. (2009). Time constraints on orogenesis from oceanic subduction to continental subduction, collision, and exhumation: an example from North Qilian and North Qaidam HP–UHP belts. *Acta Petrol. Sin.* 25 (9), 2067–2077.
- Song, S. C. (2006). Metallogenic characteristics and genetic analysis of Hongliugou Au deposit in dachaidan, Qinghai province. *West Prospect. Eng.* 18 (4), 138–140.
- Song, S. G., Zhang, L. F., Niu, Y. L., Su, L., Jian, P., and Liu, D. (2005). Geochronology of diamond-bearing zircons from garnet peridotite in the North Qaidam UHPM belt, Northern Tibetan Plateau: a record of complex histories from oceanic lithosphere subduction to continental collision. *Earth Planet. Sci. Lett.* 234 (1–2), 99–118. doi:10.1016/j.epsl.2005.02.036
- Sun, C., Yang, X., Zhang, H., Ji, W., Chen, B., Dong, Z., et al. (2022). Tracing the formation and modification of the Keketale VMS-type Pb–Zn deposit, Altai Mountains: insights from ore deposit geology, geochronology, and magnetite geochemistry. *Ore Geol. Rev.* 144, 104852. doi:10.1016/j.oregeorev.2022.104852
- Sun, G. C., Gao, P., and Zhao, Z. F. (2022). Post-collisional reworking of subducted continental crust: insights from late Paleozoic granites in the North Qaidam orogen, northeastern Tibet. *Lithos* 432, 106921. doi:10.1016/j.lithos.2022.106921
- Sun, H., Li, H., Evans, N. J., Yang, H., and Wu, P. (2017). Volcanism, mineralization and metamorphism at the Xitieshan Pb–Zn deposit, NW China: insights from zircon geochronology and geochemistry. *Ore Geol. Rev.* 88, 289–303. doi:10.1016/j.oregeorev.2017.05.010
- Sun, H. S., Li, H., Algeo, T. J., Gabo-Ratio, J. A. S., Yang, H., Wu, J. H., et al. (2019). Geochronology and geochemistry of volcanic rocks from the tanjianshan group, NW China: implications for the early palaeozoic tectonic evolution of the North Qaidam orogen. *Geol. J.* 54 (3), 1769–1796.
- Tian, J., Wang, J., Tian, T., Wang, L., Wang, Y., Yu, X., et al. (2024). *In-Situ* geochemical and Rb–Sr dating analysis of sulfides from a gold deposit offshore of Northern

- Shanshandao, Jiaodong Peninsula, North China: implications for gold mineralization. *Minerals* 14 (5), 456. doi:10.3390/min14050456
- Treloar, P. J., Lawrence, D. M., Senghor, D., Boyce, A., and Harbidge, P. (2015). The Massawa Au deposit, Eastern Senegal, West Africa: an orogenic Au deposit sourced from magmatically derived fluids? *Geol. Soc. 393* (1), 135–160. doi:10.1144/SP393.12
- Wang, G. (2012). *Geological characteristics and genesis of guolulongwa Au deposit, Qinghai province*. Changchun: Jilin University.
- Wang, L. J., Peng, Z. G., Zhu, X. Y., Deng, J. N., Wang, Y. W., and Zhu, H. P. (2009). Sources and evolution of ore-forming fluids in the Sedex-type Pb-zinc deposit, Xitie Mountain, Qinghai Province, Qinghai Province: evidence from fluid inclusions and isotopic geochemistry. *Acta Petrol. Sin.* 5 (11), 315–323.
- Wang, M., Song, S., Niu, Y., and Su, L. (2014). Post-collisional magmatism: consequences of UHPM terrane exhumation and orogen collapse, N. Qaidam UHPM belt, NW China. *Lithos* 210, 181–198. doi:10.1016/j.lithos.2014.10.006
- Wang, P., Li, Y., Zhuang, Y., Gu, P., Duan, F., Lindagato, P., et al. (2023). Middle Permian granitoids in the western section of the northern Qaidam Block, NW China: petrogenesis and tectonic implications. *J. Asian Earth Sci.* 259, 105888. doi:10.1016/j.jseaes.2023.105888
- Wang, X., Wang, Z., Zhang, W., Ma, L., Chen, W., Cai, Y. C., et al. (2024). Sulfur isotopes of lamprophyres and implications for the control of metasomatized lithospheric mantle on the giant Jiaodong gold deposits, eastern China. *Geol. Soc. Am. Bull.* 136 (7–8), 3405–3418. doi:10.1130/b37274.1
- Wu, C., Zhao, Y., Li, J., Liu, W., Zuza, A. V., Haproff, P. J., et al. (2024). Multicyclic Phanerozoic orogeny recorded in the Qaidam continent, northern Tibet: implications for the tectonic evolution of the Tethyan orogenic system. *Geol. Soc. Am. Bull.* 137 (3–4), 1553–1581. doi:10.1130/b37906.1
- Wu, C. L., Gao, Y. H., Wu, S. P., Chen, Q. L., and Joseph, F. (2007). Paleozoic granite zircon SHRIMP dating in Da chaidan area, North Qaidam. *Acta Petrol. Sin.* 23 (8), 1861–1875.
- Wu, C. L., Yang, J. S., Wooden, J., Li, H. B., and Meng, F. C. (2001). Zircon SHRIMP dating of the Qaidam mountain granite. *Sci. Bull.* 46 (20), 1743–1747.
- Xia, R., Deng, J., Qing, M., Wang, C. M., and Li, W. L. (2013). The genesis of the Dachang Au ore field in Qinghai Province: constraints on fluid inclusion geochemistry and H-O isotopes. *Acta Petrol. Sin.* 29 (4), 1358–1376.
- Xu, G. D. (2012). *Study on the genesis of the shuangkoushan Pb-zinc deposit in Dachaidan, Qinghai province*. Wuhan: University of Geosciences.
- Xu, N., Li, S., Wu, C., and Santosh, M. (2019). Geochemistry and geochronology of the Dongyang gold deposit in southeast China: constraints on ore genesis. *Geol. J.* 55 (1), 425–438. doi:10.1002/gj.3421
- Xu, Z. Q., Yang, J. S., Wu, C. L., Li, H. B., Zhang, J. X., Qi, X. X., et al. (2003). The time limit and mechanism of formation and exhumation of ultra - high pressure metamorphic belt in North Qaidam. *Geology* 77 (2), 163–176.
- Xue, C. Y. (2011). *Metallogenic fluid characteristics of Au deposit in xincheng, jiaodong*. Beijing: China University of Geosciences.
- Yang, C. X., and Santosh, M. (2020). Ancient deep roots for Mesozoic world-class gold deposits in the north China craton: an integrated genetic perspective. *Geosci. Front.* 11 (1), 203–214. doi:10.1016/j.gsf.2019.03.002
- Yardley, B. W. D., and Cleverley, J. S. (2015). The role of metamorphic fluids in the formation of ore deposits. *Geol. Soc. Lond. Spec. Publ.* 393 (1), 117–134. doi:10.1144/sp393.5
- Yoo, B., and White, N. (2013). Mineralogy, fluid inclusion and stable isotope constraints on the genesis of the namseong au-ag deposit, Republic of Korea. *Geochem. J.* 47 (3), 285–307. doi:10.2343/geochemj.2.0245
- Yu, F. C., Ma, G. L., Wei, G. F., Wang, Y. X., and Mei, A. J. (1998). Analysis of geological characteristics and ore-controlling factors of the Tanjianshan Au deposit, Qinghai Province. *Ore Depos.* 17 (1), 47–56.
- Yu, J. Z., Zheng, Y. Y., and Xu, R. K. (2020). LA-ICP-MS zircon U-Pb age of the host rock and hydrothermal zircon in gold-bearing quartz vein of Shuangkoushan Au-Ag-Pb deposit, north Qaidam: limitation for the mineralization age and implication for the Genesis of the deposit. *Acta Geol. Sin.* 94 (11), 3361–3375.
- Zhang, B., He, M., Hang, W., and Huang, B. (2013). Minimizing matrix effect by femtosecond laser ablation and ionization in elemental determination. *Anal. Chem.* 85, 4507–4511. doi:10.1021/ac400072j
- Zhang, B. W., Sun, F. Y., Xue, H. R., and Wang, L. (2010). Geological characteristics and fluid inclusions of Qinglonggou Au deposit, Qinghai. *Au Mag.* 31 (2), 14–18.
- Zhang, D. Q., Dang, X. Y., She, H. Q., Li, D. X., Feng, C. Y., and Li, J. W. (2005). Ar–Ar dating and its geological significance of orogenic gold deposits in northern margin of Qaidam and East Kunlun. *Mineral. Deposits* 24 (3), 87–98.
- Zhang, D. Q., Feng, C. Y., Li, D. X., Xu, W. Y., Yan, S. H., Yu, H. Q., et al. (2001). Orogenic Au deposits in the North Qaidam and East Kunlun orogen, west China. *Depos. Geol.* 20 (2), 137–146.
- Zhang, D. Q., Zhang, H., Feng, C. Y., Yu, H. Q., Li, J. W., and Li, D. X. (2007). Multiple Au mineralization in Tanjianshan Au deposit: evidence from fluid inclusions. *Depos. Geol.* 26 (5), 519–526.
- Zhang, G. B., Song, S., Zhang, L., and Niu, Y. (2008). The subducted oceanic crust within continental-type UHP metamorphic belt in the North Qaidam, NW China: evidence from petrology, geochemistry, and geochronology. *Lithos* 104 (1–4), 99–118. doi:10.1016/j.lithos.2007.12.001
- Zhang, L. C., Ji, J. S., Li, H. Q., and Shen, Y. C. (2000). Geochemical characteristics and source of two-type ore-forming fluids in Kanggultage Au ore belt, east Tianshan. *Acta Petrol. Sin.* 16, 535–541.
- Zhang, W., Hu, Z., and Liu, Y. (2020). Iso-Compass: new freeware software for isotopic data reduction of LA MC-ICP-MS. *J. Anal. Atomic Spectrom.* 35, 1087–1096. doi:10.1039/D0JA00084A
- Zhang, X. P., Wang, Q. F., Hui, J., Chang, X., and Tong, H. K. (2015). Chemical characteristics of volcanic rocks from the Tanjianshan Group on the northern margin of the Qaidam basin and its tectonic environment. *J. Mineralogy Petrology* 35 (1), 18–26.
- Zhang, Y. (2011). *Metallization of aialongwa carlin-like Au deposit in ganzhi-litang suture zone, West Sichuan province*. Beijing: China University of Geosciences.
- Zhao, F. Q., Guo, J. J., and Li, H. K. (2003). The geological characteristics and isotopic chronology of the Tanjianshan group in Xitieshan region, Qinghai province. *Geol. Bull.* 22 (1), 28–31.
- Zhao, H. X. (2011). *Study on mineralization geochemistry of Au deposit in Xiaqinglin*. Nanjing: Nanjing University, 74–82.
- Zheng, Y. F., and Chen, J. F. (2000). *Stable isotope geochemistry*. Beijing: Science Press.
- Zhu, X. H., Chen, D. L., Wang, C., Wang, H., and Liu, L. (2015). The initiation, development and termination of the neoproterozoic-early paleozoic ocean in the northern margin of Qaidam basin. *Acta Geol. Sin.* 89 (2), 234–251.
- Zhu, X. Y., Wang, L. J., Zhu, G. D., Deng, J. N., Fan, J. C., and Zhang, Q. (2010). Study on source of ore-forming materials in Xitieshan SEDEX Pb-zinc deposit: evidence from Pb isotope geochemical. *Geol. China* 37 (6), 1682–1689.
- Zoheir, B. A., Johnson, P. R., Goldfarb, R. J., and Klemm, D. D. (2019). Orogenic gold in the Egyptian Eastern Desert: widespread gold mineralization in the late stages of Neoproterozoic orogeny. *Gondwana Res.* 75, 184–217. doi:10.1016/j.gr.2019.06.002
- Zong, K. Q., Klemd, R., Yuan, Y., He, Z. Y., Guo, J. L., Shi, X. L., et al. (2017). The assembly of Rodinia: the correlation of early Neoproterozoic (ca. 900 Ma) high-grade metamorphism and continental arc formation in the southern Beishan Orogen, southern Central Asian Orogenic Belt (CAOB). *Precambrian Res.* 290, 32–48. doi:10.1016/j.precamres.2016.12.010